

HIRMES – High Resolution Mid-infrared Spectrometer

PI: Harvey Moseley

Deputy PI: Alexander Kuttyrev

Project Manager: Wen-Ting Hsieh

System Engineer: Leroy Sparr

Science team:

E. Bergin (Univ. of Michigan)

G. Bjoraker (GSFC)

G. Melnick (SAO)

S. Milam (GSFC)

D. Neufeld (JHU)

K. Pontoppidan (JHU)

S. Rinehart (GSFC)

A. Roberge (GSFC)

G. Stacey (Cornell University)

J. Staguhn (JHU/GSFC)

D. Watson (Rochester)



What is HIRMES?

- HIRMES is the recently selected 3rd generation instrument that will fly on SOFIA in early 2019
- HIRMES primary science is to investigate protoplanetary disk physics and addresses the questions:
 - How does the disk mass evolve during planetary formation?
 - What is the distribution of oxygen, water ice, and water vapor in different phases of planet formation?
 - What are the kinematics of water vapor and oxygen in protoplanetary disks?

Over riding theme is discover how protoplanetary systems evolve

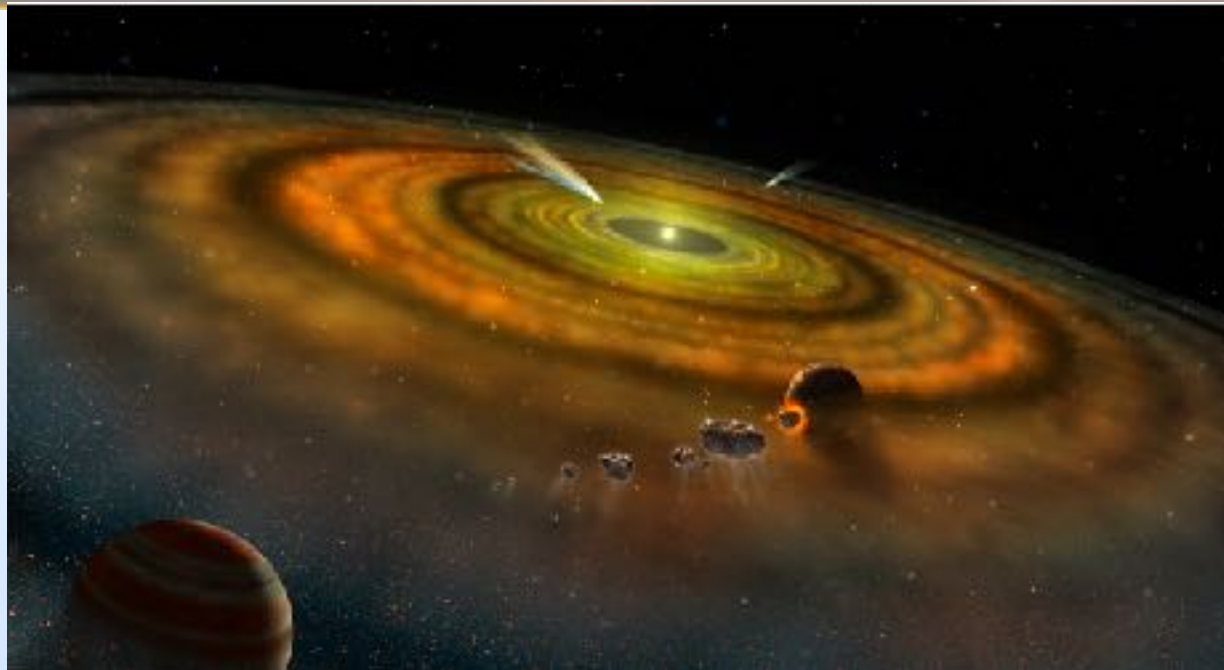


How is the Science Achieved

- HIRMES is a direct detection spectrometer covering the spectral range from 25 to 122 μm
- There are four spectroscopic modes to HIRMES
 - High-res mode $R \sim 100,000$
 - Mid-res mode $R \sim 10,000$
 - Low-res mode $R \sim 600$
 - Imaging spectroscopy mode: $R \sim 2000$
- The modes are optimized to deliver the maximum sensitivity achievable with SOFIA. HIRMES uses:
 - Background limited bolometers
 - Combination of Fabry-Perot Interferometers and gratings



Primary Science



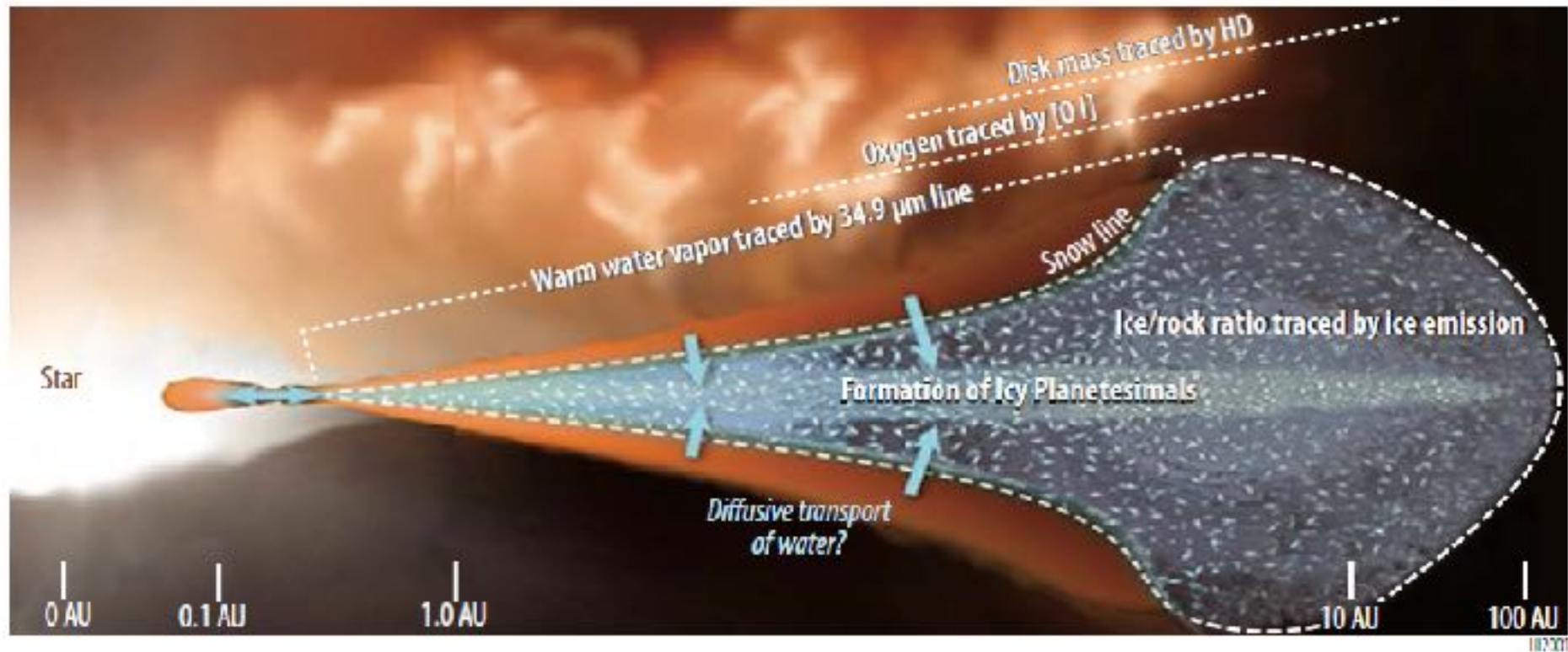
- Over ~ 10 million years, protoplanetary disks evolve into young planetary systems
- Bulk of mass is gas and ice – both hard to observe
- Hinders testing & development of planet formation theories

HIRMES and Protoplanetary Disks

- **Water and ice:** water and ice play a critical role in the formation of giant planet cores and, producing habitable conditions in terrestrial planets
 - H₂O 34.9823 μm 651-624 rotational line
 - Ice 43, 47, 63 μm
- **Neutral Oxygen:** a tracer of disk chemistry and radial structure
 - [OI] 63.1837 μm $^2\text{P}_1$ - $^3\text{P}_2$ fine-structure line
- **Deuterated hydrogen:** a tracer of disk mass
 - HD 112.0725 μm J = 2-0 rotational line
 - HIRMES resolves these narrow lines and determines their origins from velocity profiles



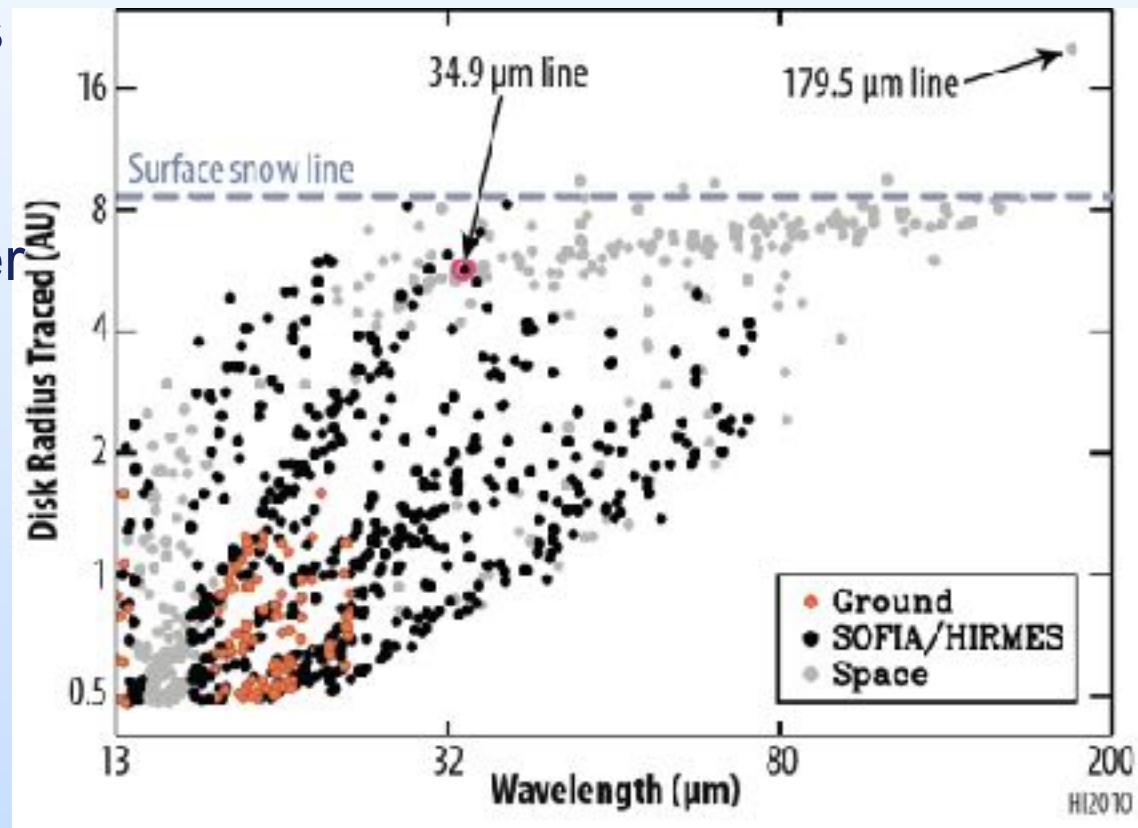
Water and Ice



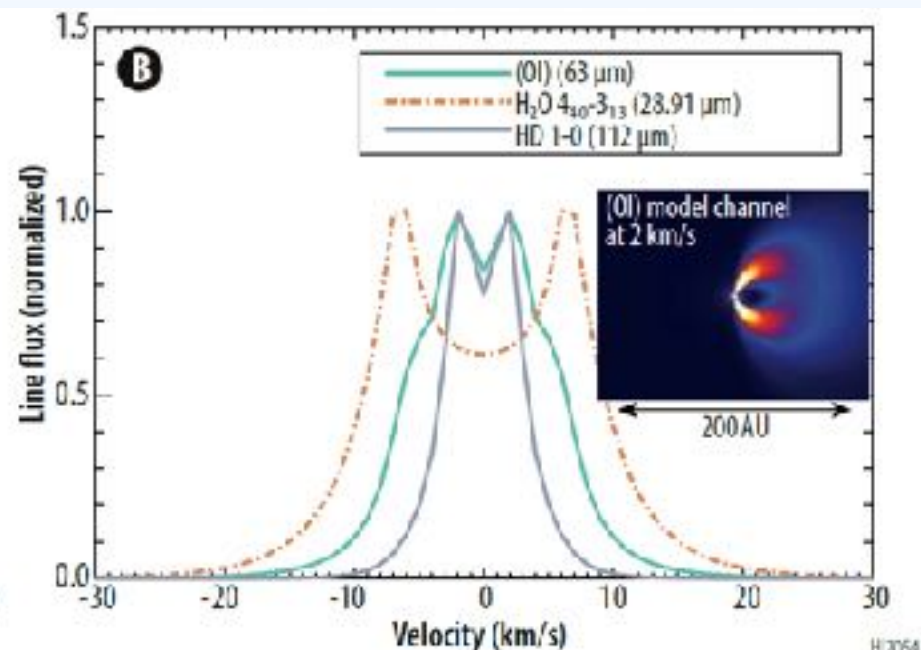
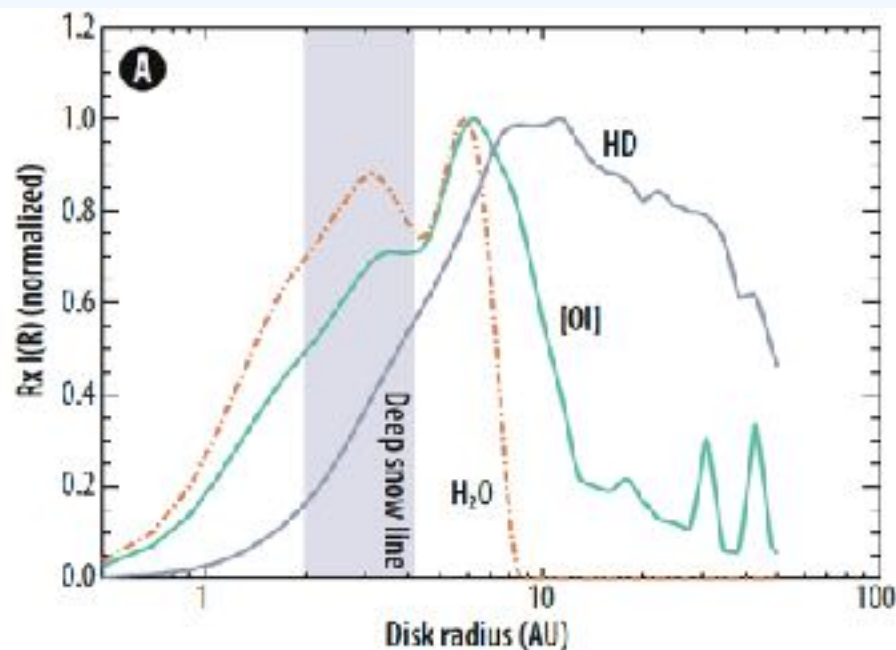
Water line measurements locate the transition region between warm water vapor and ice through velocity resolved spectroscopy

HIRMES Traces Water at the Snow Line

- Ground based lines probe very inner regions
- Space based can probe entire disk, but will not have the resolving power
- HIRMES probes out to the snow line regions at ~ 10 AU with sufficient velocity resolution and sensitivity to constrain models



Distributions of O, H₂O and HD



- Measuring the line profiles determines the radial distributions of O, H₂O and HD in the disk
- O and H₂O are expected to be in and around the snow line while HD is external ⇒ HD requires less RP than O and H₂O observations



Ice Diagnostics

- Detect ice through its crystalline (43 and 63 μm) and amorphous (47 μm) ice features
- The far-IR has unique tracers of ice, since ice warm enough to emit in its shorter wavelength bands will melt
- Emission arises from small icy grains above the colder disk
- Strength of features yields mass of ice
- Ice features not available to other facilities so this is not well explored observationally

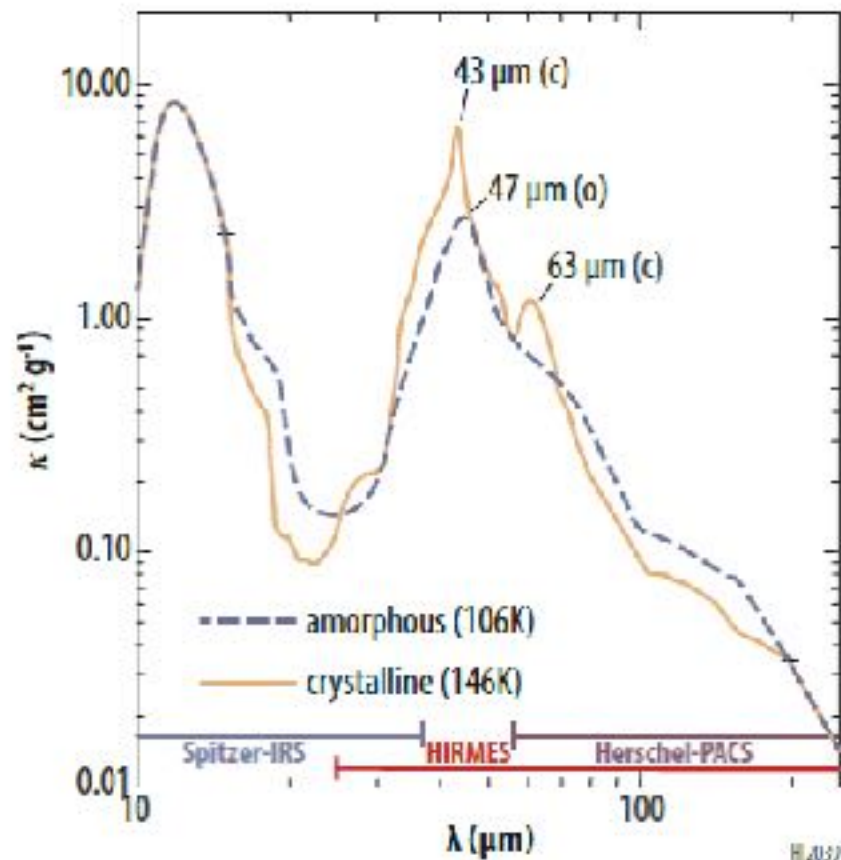


Figure D-4: HIRMES can infer the thermal history of grain mantles by observation of the 43, 47 and 63 μm water-ice features. The plot shows the emission/absorption coefficients (McClure et al. 2015).

The Impact of Star Formation

- The process of mass accretion leading to star and planet formation involves shocks that release refractories and can result in ionized gas emission lines
- [SI] 25.25 μm ; [FeII] 25.99, 35.35 μm , [SIII] 33.48 μm , [SIII] 34.81 μm ; [NeIII] 36.0 μm , [OIII] 51.81 μm , [NIII] 57.30 μm , [OI] 63.18 μm , [OIII] 88.35 μm
- Lines and ratios reveal gas abundances, ionization state, and density testing shock models and mass flow models
- The velocity resolved line profiles reveal the shocked gas kinematics
- Herschel and Spitzer did trace intensity and spatial profiles, but the spectral profiles are key components of shock models



Further Shopping List

High velocity resolution and high sensitivity of HIRMES enables much new science

- Outflows from massive protostars traced with CO
- HD as a probe of D abundance
- Resolved HD rotational lines from giant planets
- Titan chemistry
- ...
- Imaging spectroscopy mode with its wide field of view enables large-scale mapping of nearby galaxies in fine-structure line emission



Sensitivity Estimates in Hi-Res Mode

Line/ λ (μm)	V_{obs} (km/s)	Pixel	η_{atm}	NEP (W/Hz ^{1/2})	η_{pix}	NEF (W/m ² /Hz ^{1/2})	MDLF (W/m ² , 5 σ /hr)
H ₂ O 34.9823 μm	-40	2.9"	94%	1.35E-17	60%	2.4E-17	1.4E-18
	+20		84%	2.24E-17		4.4E-17	2.6E-18
	+40		93%	1.35E-17		2.4E-17	1.4E-18
[OI] 63.1837 μm	-40	5.2"	65%	1.37E-17	60%	3.6E-17	2.1E-18
	0		62%	1.45E-17		4.2E-17	2.3E-18
	+40		59%	1.45E-17		4.2E-17	2.5E-18
HD 112.0725 μm	-40	9.2"	58%	9.47E-18	60%	2.9E-17	1.7E-18
	0		58%	9.49E-18		2.9E-17	1.7E-18
	+40		56%	9.67E-18		3.1E-17	1.8E-18

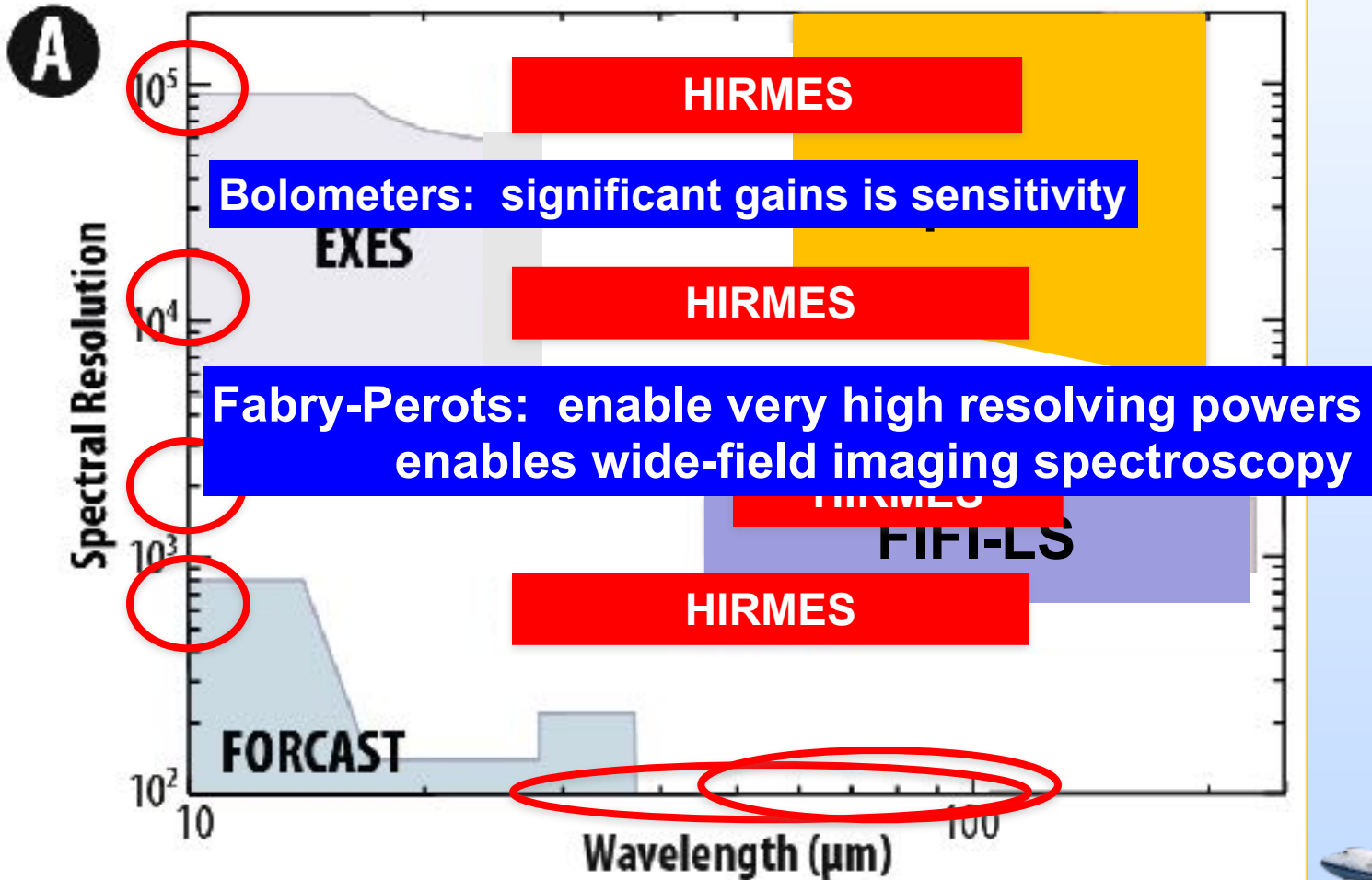


SNR Estimates: HD163296

Line	Flux	MDLF	SNR if line width is:			
Line	Flux	MDLF	0 km/s	3 km/s	6 km/s	15 km/s 0.5 hours/samp.
H ₂ O	3.1E-17	1.97E-18 RP = 50,000	75 (1 hr)		75 (5 hrs)	50 (5 hours)
		1.40E-18 RP = 100,000	110 (1 hr)	114 (3 hrs)	100 (5 hrs)	50 (5.5 hours)
[OI]	2.1E-16	3.50E-18 RP = 50,000	300 (1 hr)		220 (1 hrs)	90 (1 hours)
		2.49E-18 RP = 100,000	420 (1 hr)	260 (1 hrs)	175 (1 hr)	85 (1 hours)
HD	1.0E-17	2.55E-18 RP = 50,000	20 (1 hr)		21 (3 hrs)	16 (5 hours)
		1.82E-18 RP = 100,000	27 (1 hr)	29 (3 hrs)	25 (5 hrs)	15 (5 hours)



HIRMES in SOFIA Context



Comparison with upGreat

- Coherent detection fundamentally limited in sensitivity by the quantum noise limit inherent in the detection of phase and manifest as: $T_{QN} = \frac{h\nu}{k}$

Sensitivity ratio estimates based on public upGREAT sensitivities:

[OI] 63 μm 10:1

HD 112 μm 10:1

$T_{rec} \sim 590 \text{ K} @ 122 \mu\text{m} \rightarrow 2770 @ 26 \mu\text{m}$ single side band

- The sky plus telescope emissivity is $\sim 20\%$ so the fundamental limits are $T_{rec} \sim 0.2 \cdot 240 = 48 \text{ K}$
- Direct detection in principle wins by factors of 12 (122 μm) to 58 (26 μm) over coherent detection



Comparisons with FIFI-LS

- Both are direct detection spectrometers, so they do not suffer from quantum noise limit
 - However, bolometers have two advantages over photoconductors
 - Bolometers can have >90% quantum efficiency over reasonably broad bands
 - Bolometers do not have generation recombination noise
- Penalty for FIFI-LS is $\sim \sqrt{(0.95/0.5)} \times \sqrt{2} \sim 2$ in sensitivity***
- FIFI-LS is a spectral multiplexer, but HIRMES is not
- Penalty for HIRMES = $\sqrt{5} \sim 2.23$ (res. el.) in sensitivity***

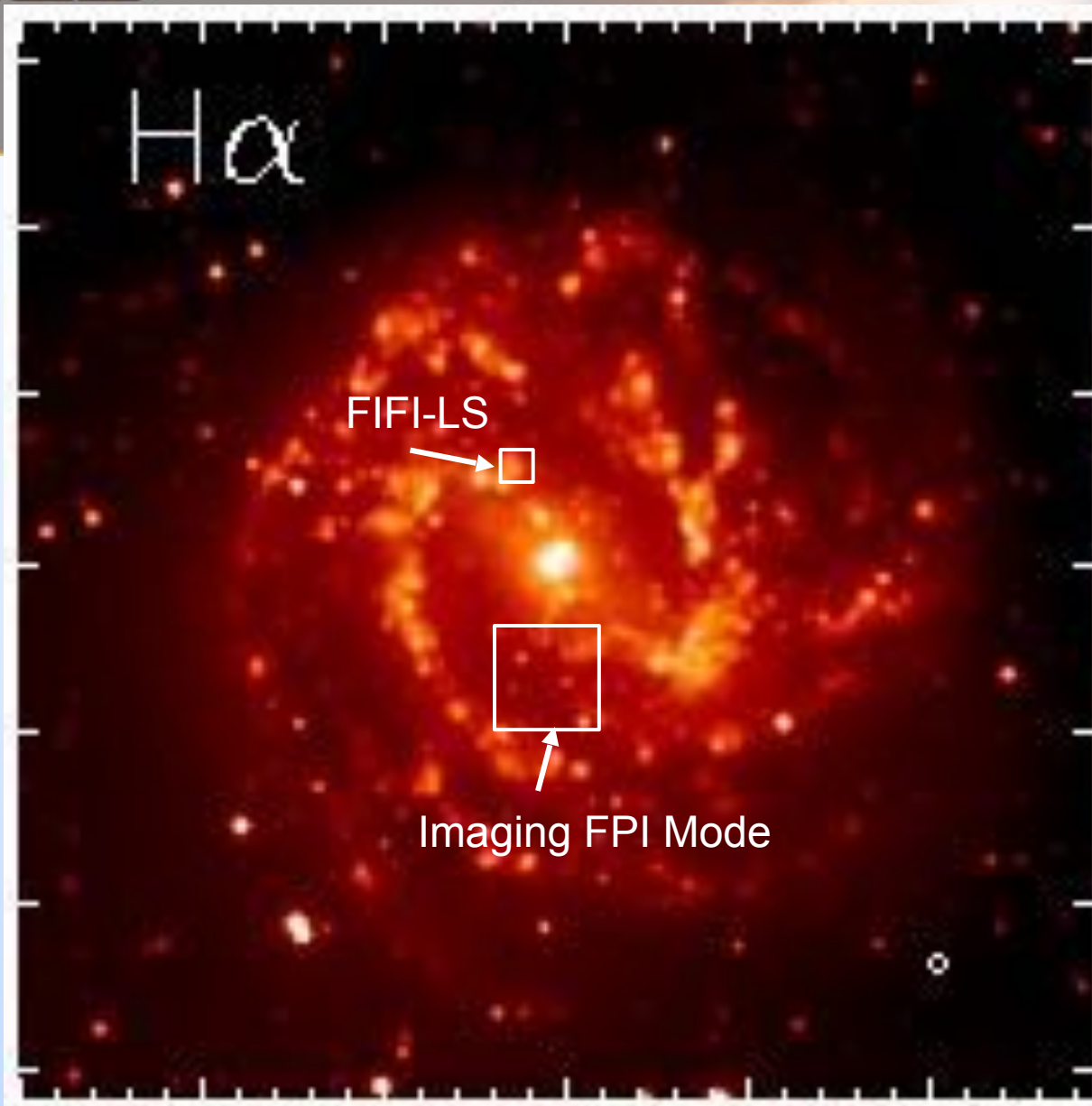


Imaging Mode Mapping Speed

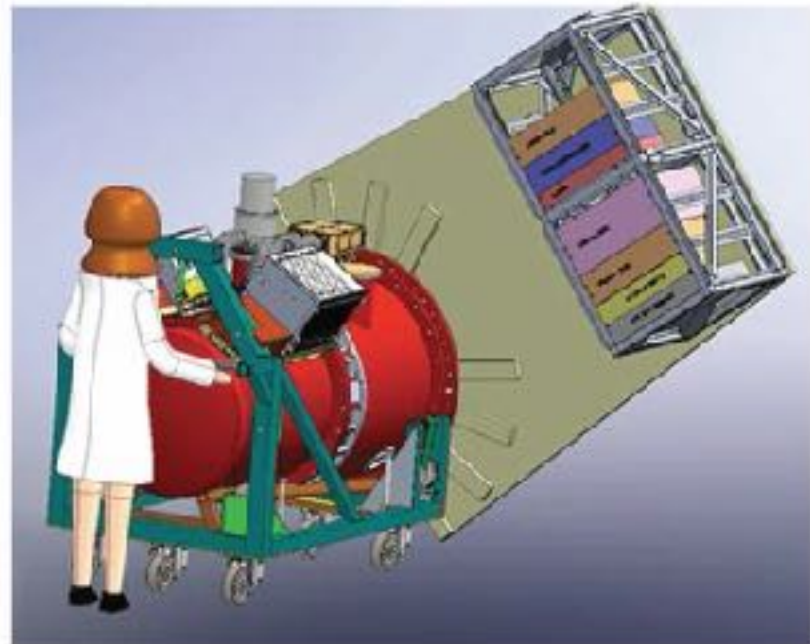
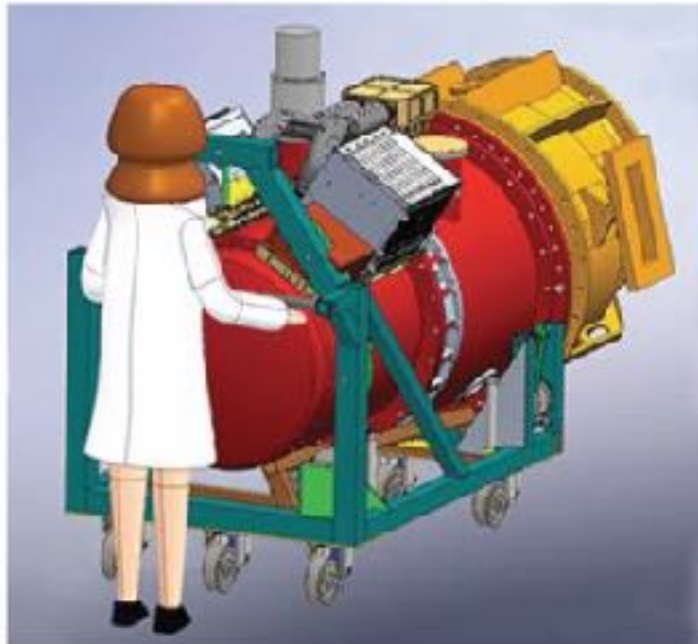
Line	FIFI-LS	HIRMES	Sens. Ratio	Sky Sub.	FPI Scan	Net Sens	Areal Cover.	Mapping Speed
[OIII] 51.8 μm	5.4E-17	2.0E-17	0.36	0.84	2.23	0.69	10.6	22
[NIII] 57.3 μm	5.1E-17	2.1E-17	0.41	0.84	2.23	0.77	10.6	18
[OI] 63.2 μm	6.4E-17	3.3E-17	0.52	0.84	2.23	0.98	10.6	11
[OIII] 88.4 μm	4.3E-17	0.76E-17	0.18	0.84	2.23	0.33	10.6	95
[NII] 122 μm	6.9E-17	1.2E-17	0.18	0.84	2.23	0.34	2.6	23

NOTES: FL = 41,000', $v = 0$ km/s except for [NII] @ 43,000', $v = 520$ km/s; source el. = 45°; MDLF = 4σ , 15 minutes; sky sub. = 1.7 (FIFI), 1.1 (HIRMES)





HIRMES on the Outside

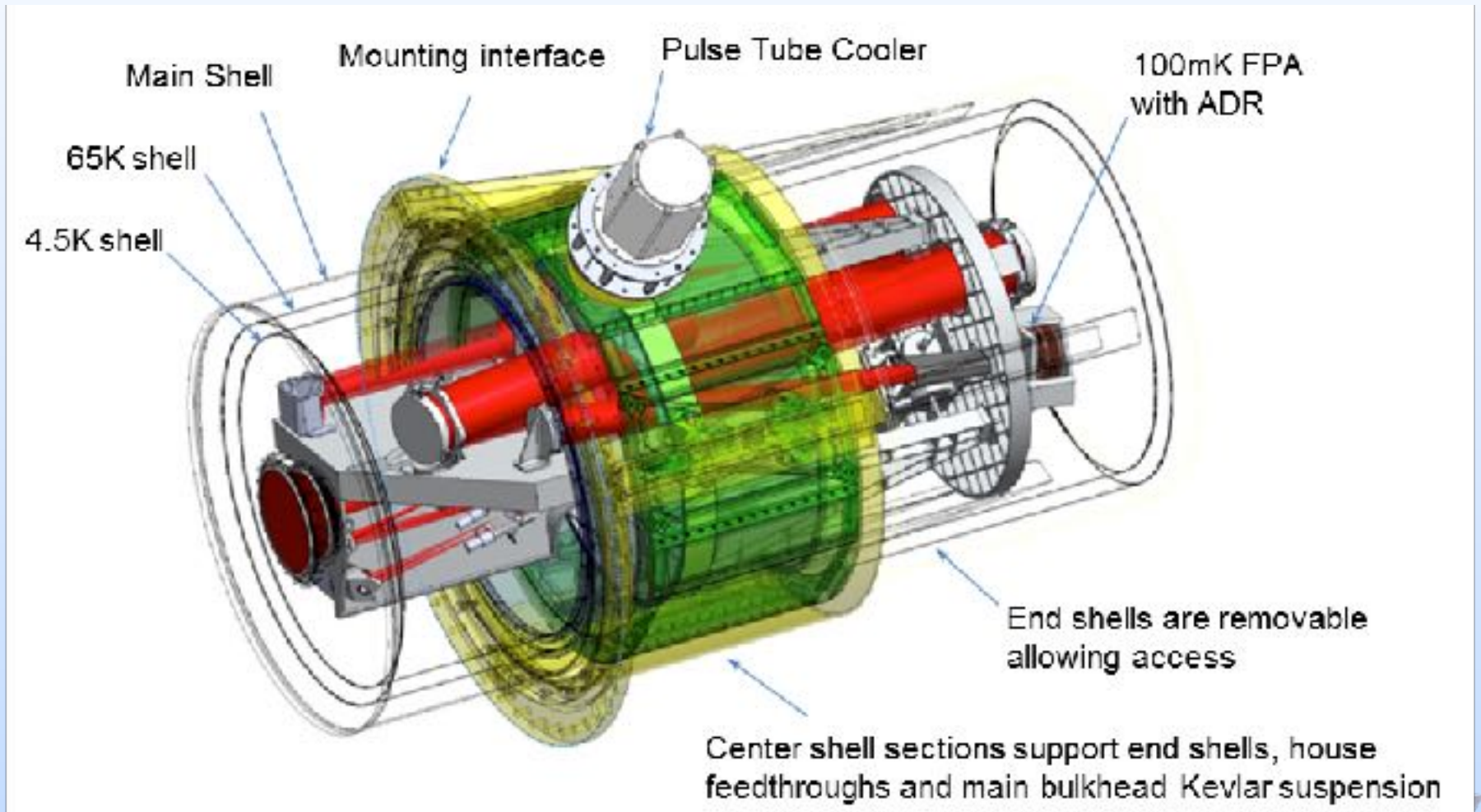


HRO:7

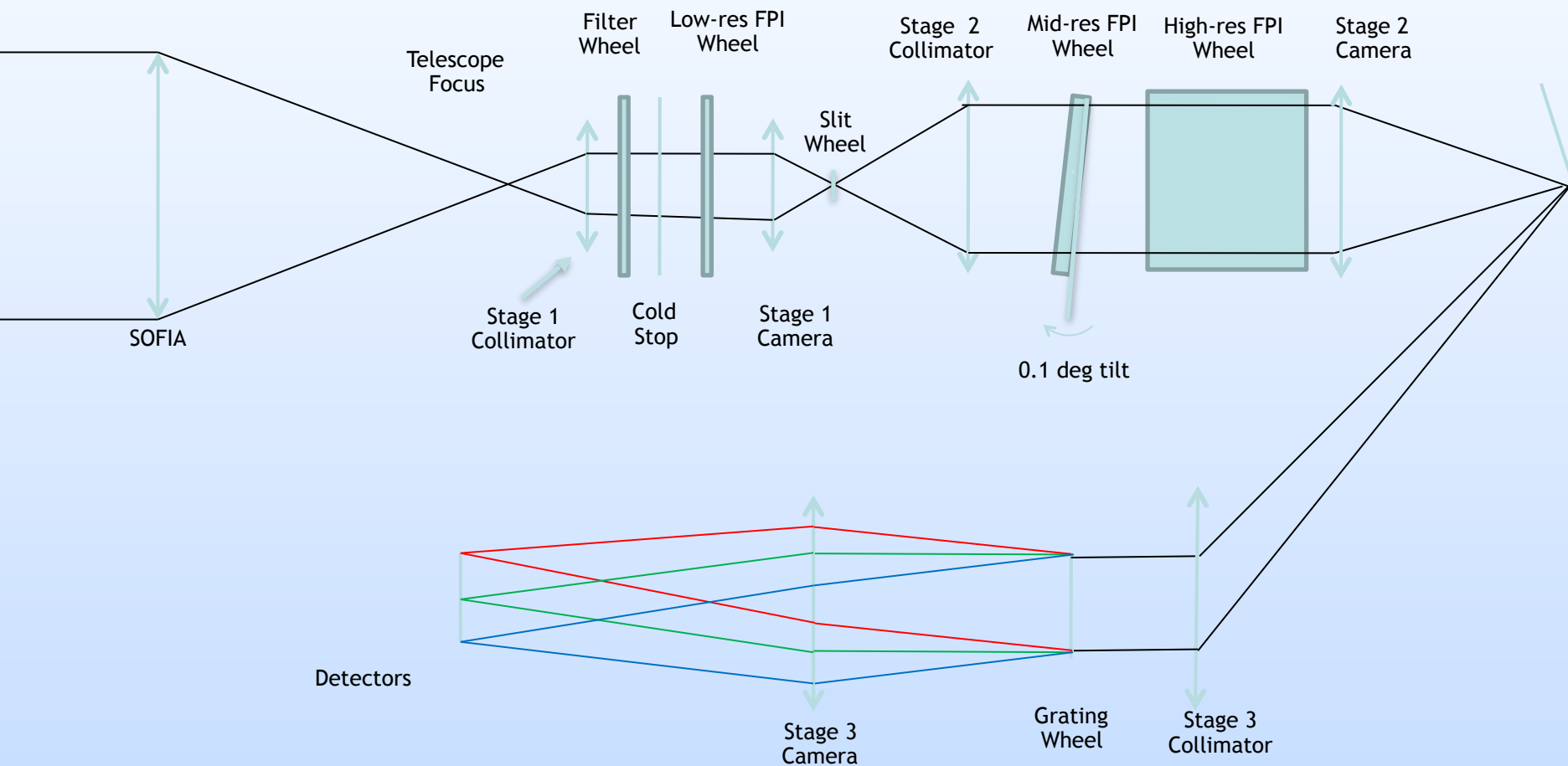
Figure E-4: Left: HIRMES on installation cart; Right: HIRMES and CWR installed on TA.



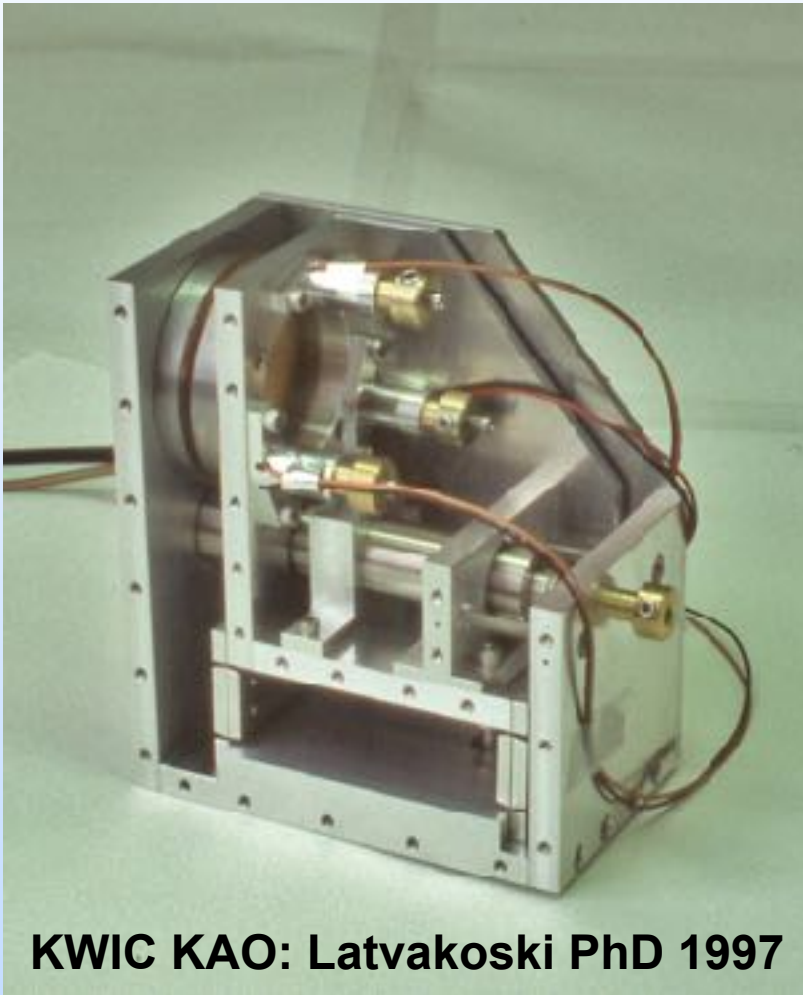
HIRMES Interior



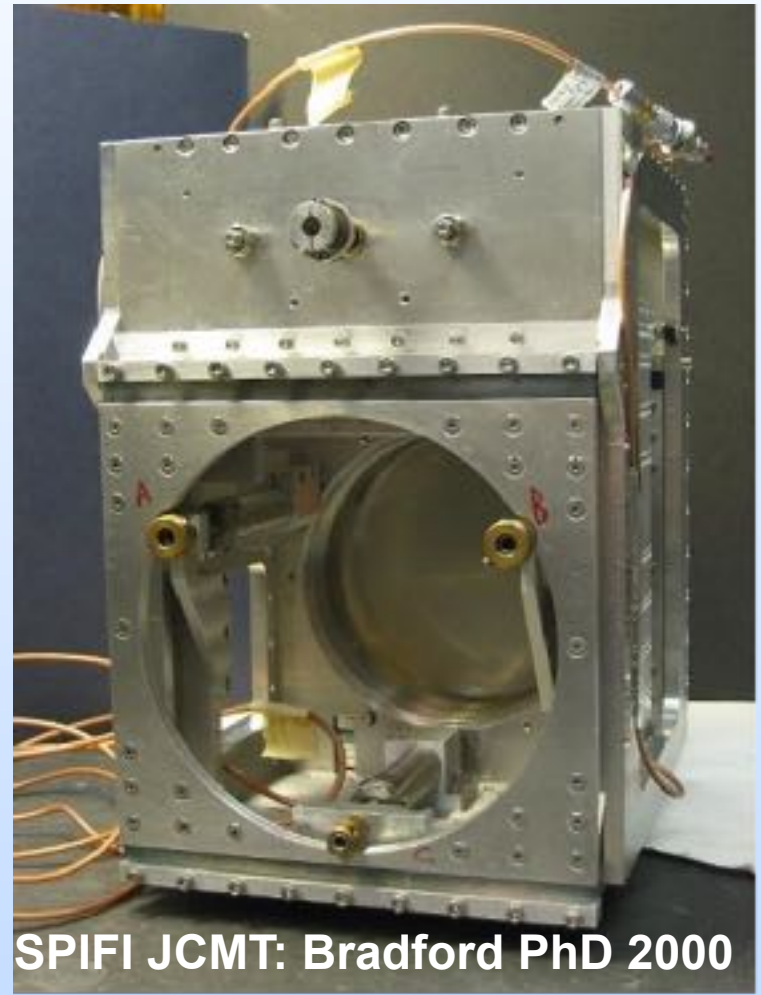
Schematic Optical Path



Scanning FPI Examples



KWIC KAO: Latvakoski PhD 1997



SPIFI JCMT: Bradford PhD 2000

Scanning FPI Designs

- Wire EDM manufacture
- Fixed order, PZT drive
- Capacitive bridge control
- Metal mesh mirrors
- 3 Hi-res; 3 Mid-res

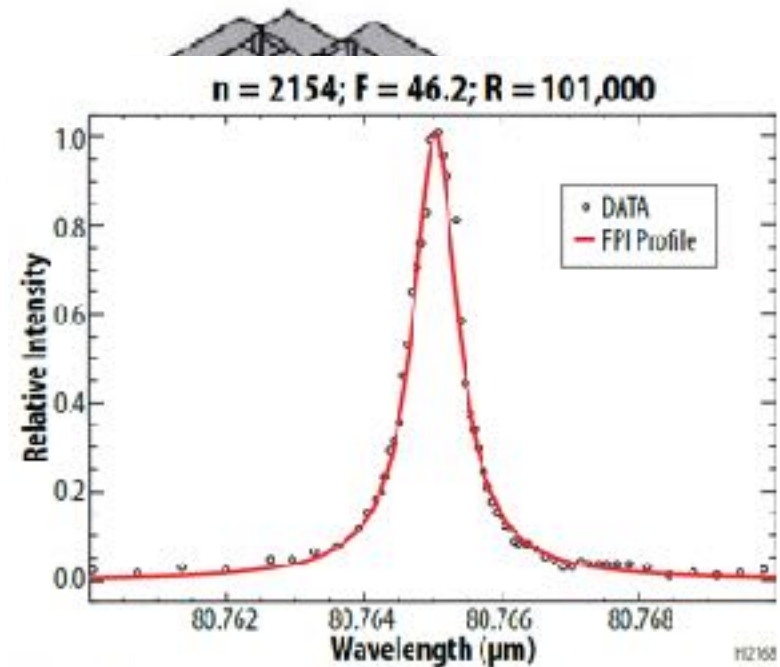
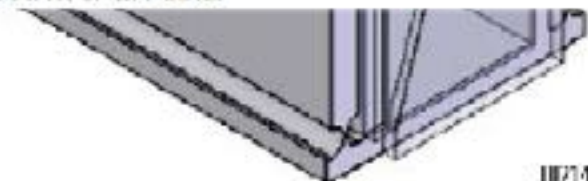


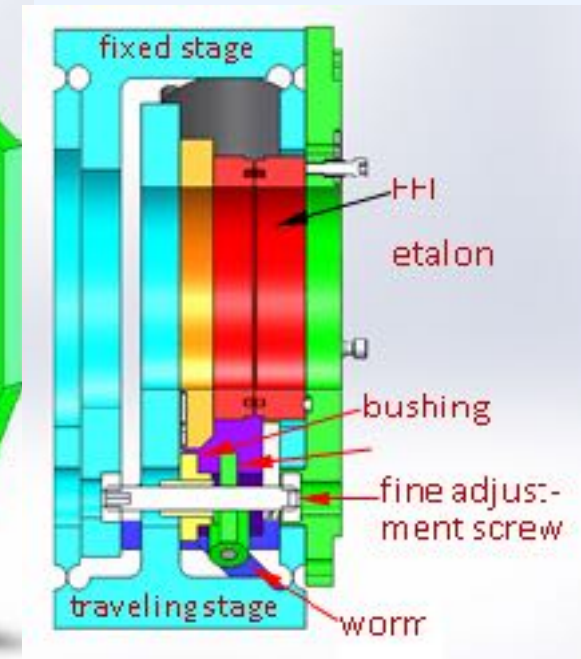
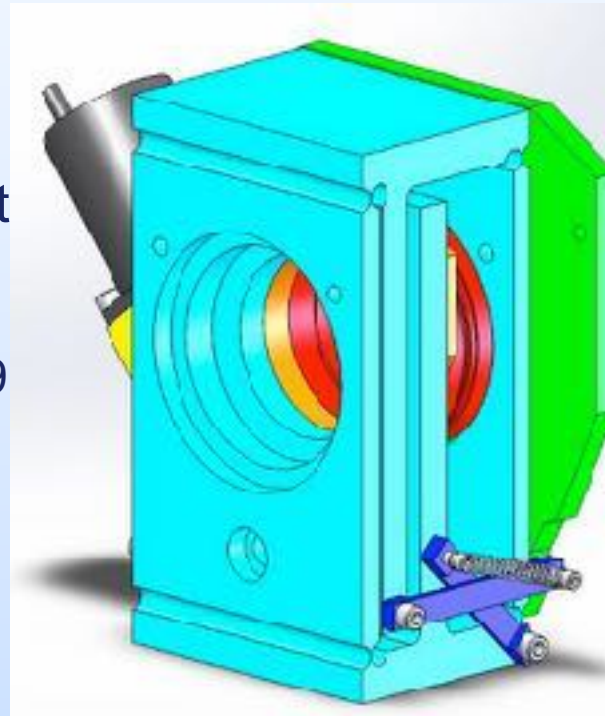
Figure E-18: Recent demonstration of a resolving power of 101,000 obtained by scanning a test-bed FPI interferometer across a 80.765 μm quantum cascade laser line. The theoretical profile is a good fit to the data.



Low-Res Imaging FPI

Based on Miniature Cryogenic Scanning FPI Design

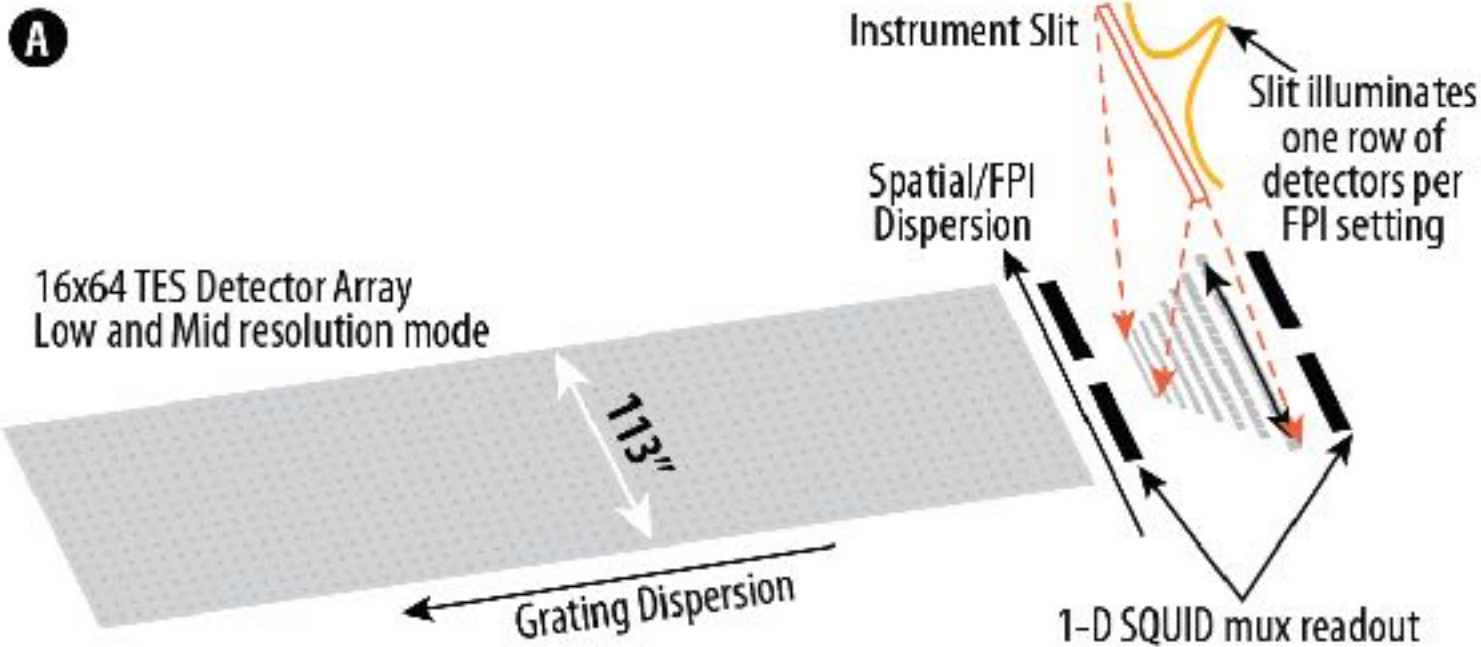
- Two Imaging FPI required
- Fix order for R.P. = 2000 at band center
- Imaging FPI -1
 - $F = 41 @ 57 \mu\text{m} \Rightarrow m = 49$
 - $F = 50 @ 63 \mu\text{m} \Rightarrow \text{RP} = 2200$
 - $F = 34 @ 52 \mu\text{m} \Rightarrow \text{RP} = 1810$
- Imaging FPI -2
 - $F = 60 @ 122 \mu\text{m} \Rightarrow \text{R.P.} = 2260$
 - $F = 31 @ 88 \mu\text{m} \Rightarrow \text{R.P.} = 1630$



Wire EDM eliminates need for tilt PZTs



Bolometer Arrays



Pixel scales

Array 1:

6.1×6.1"

No back short ⇒ very broad band response

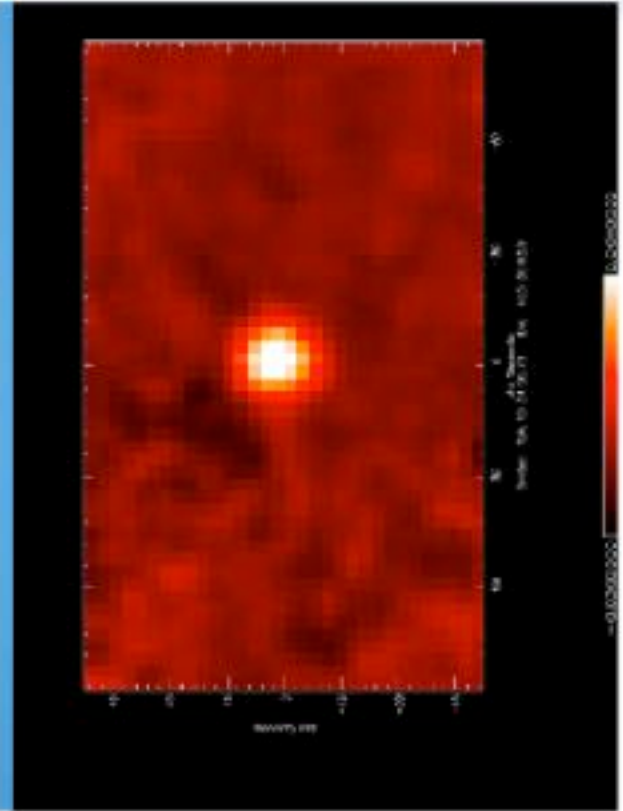
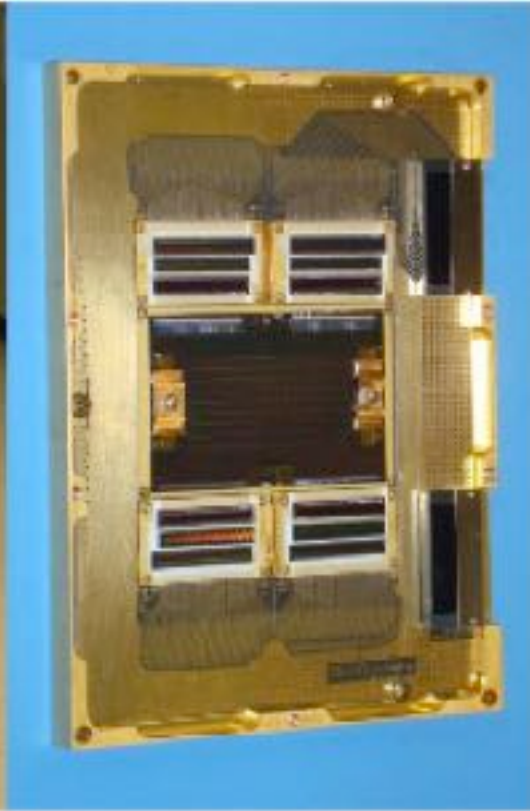
Array 2:

2.5 to 8.5"

Back short tuned

- Two MoAu TES bolometer arrays are used within HIRMES
 - 16 × 64 pixel array used for low-res (grating) mode, mid-res mode, and imaging spectroscopy mode
 - 8 × 16 pixel array used for high-res mode

Heritage: GISMO (J. Staguhn)



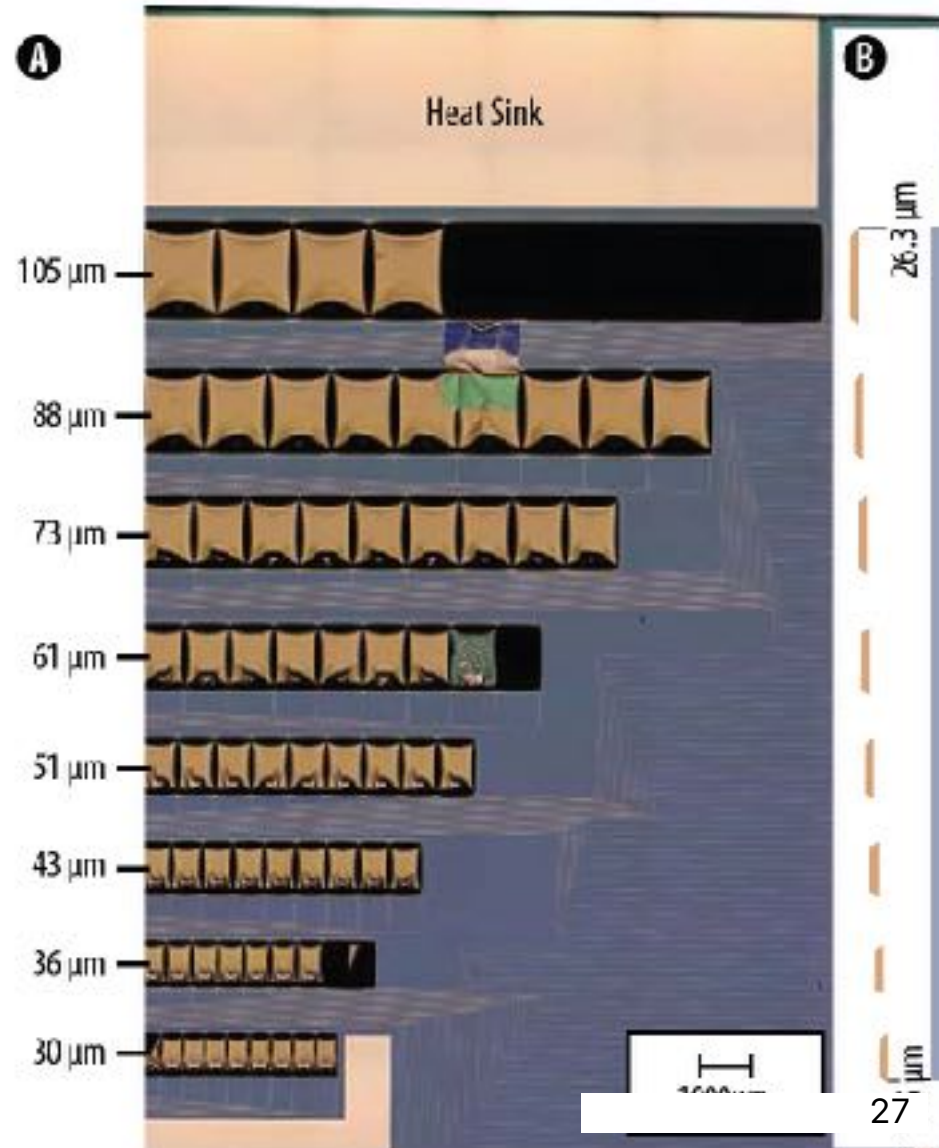
GISMO instrument (left), center – detector assembly, right - image of Arp 220 - ULIRG. GISMO is being operated at IRAM 30m sub-mm telescope for a number of years.



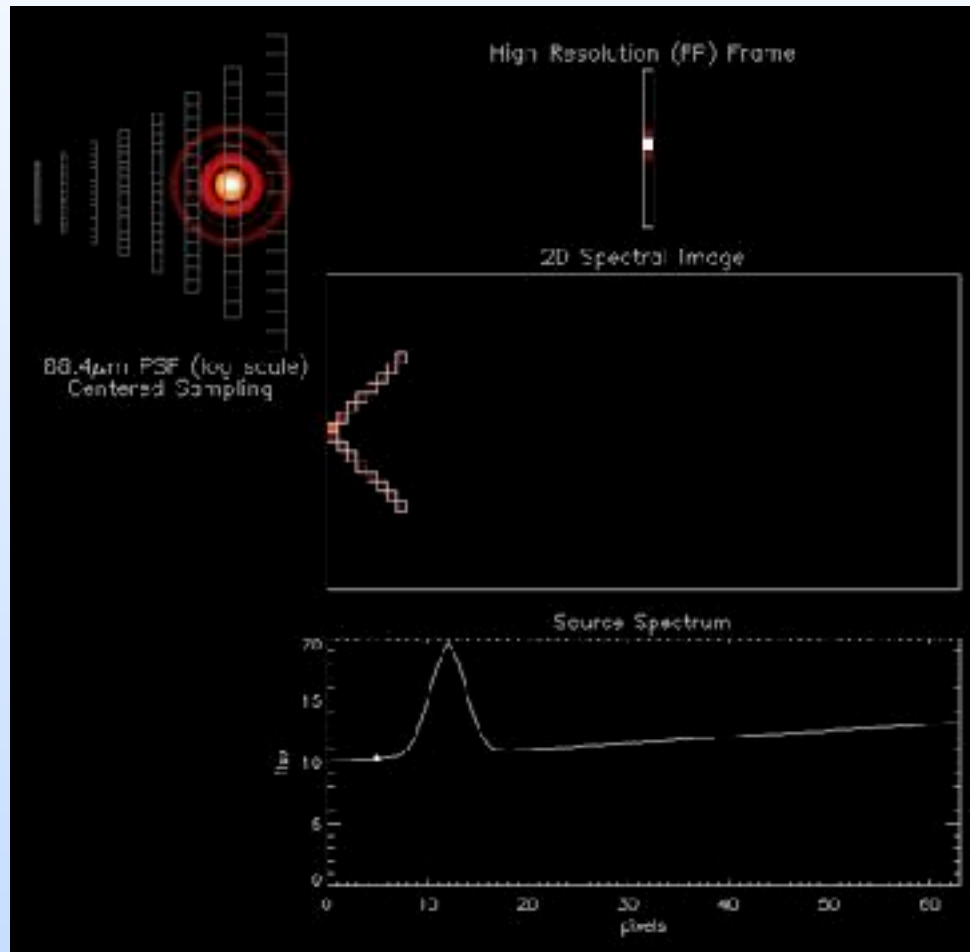
Array Development

8 × 16 array

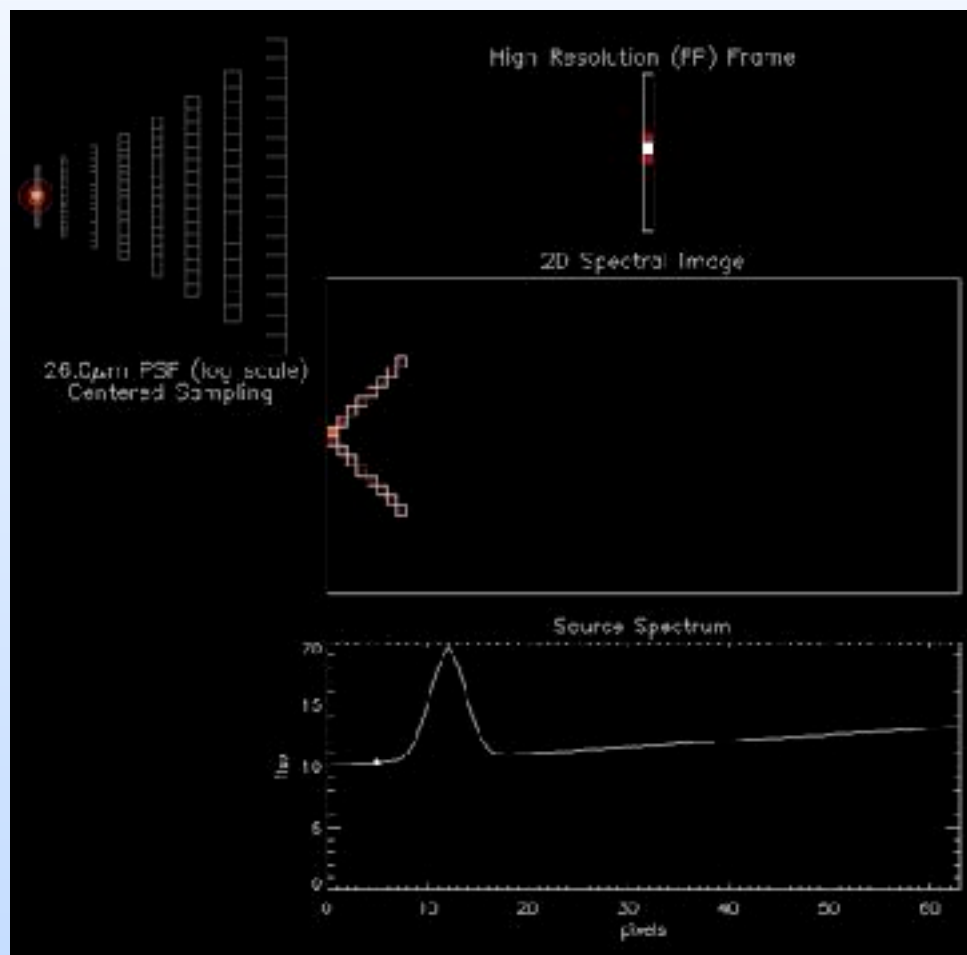
- Pixel scale always λ/D for optimal sensitivity
 - Optimal signal/pixel vs noise/pixel extraction for point sources
 - Minimizes aberrations and spectral shifts for high-res spectra
- Each array tuned with back short at center of band \Rightarrow DQE > 90%
- Requisite sensitivity demonstrated at GSFC



Building the Hi-Res Spectrum



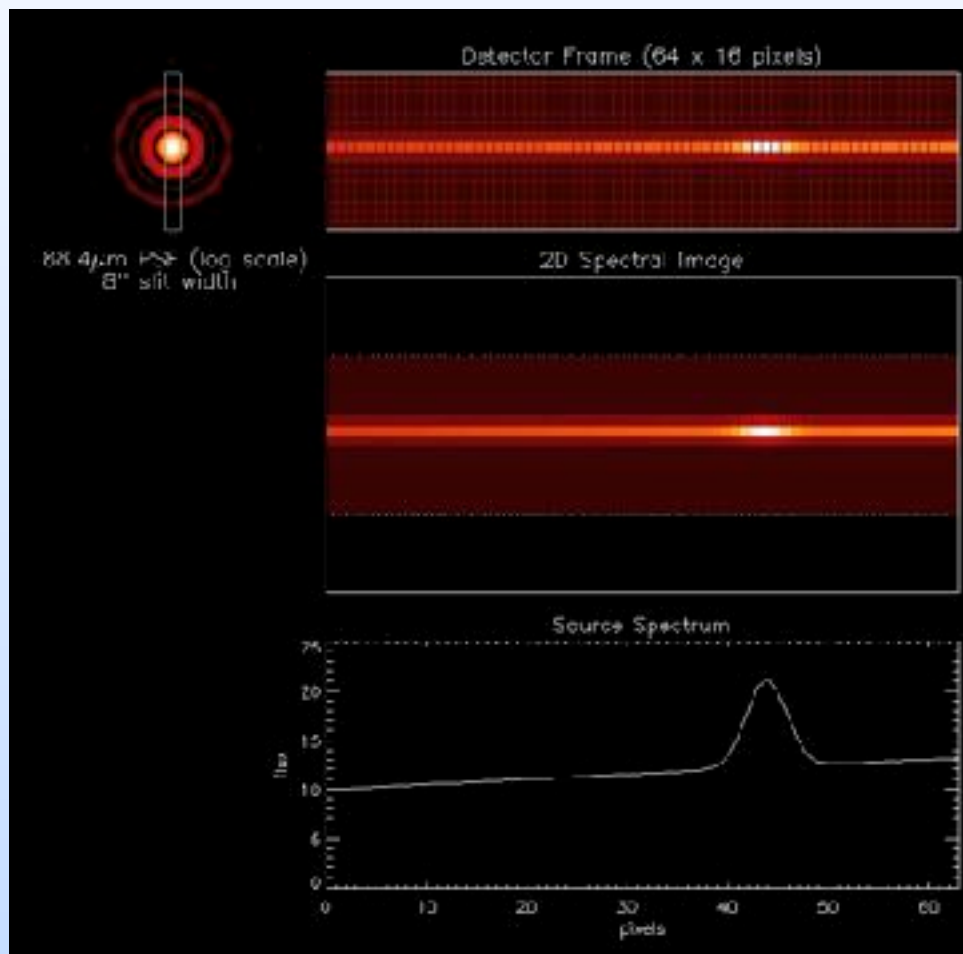
26 μm High-Res



The Local Truth: Star Formation and Feedback in the SOFIA Era



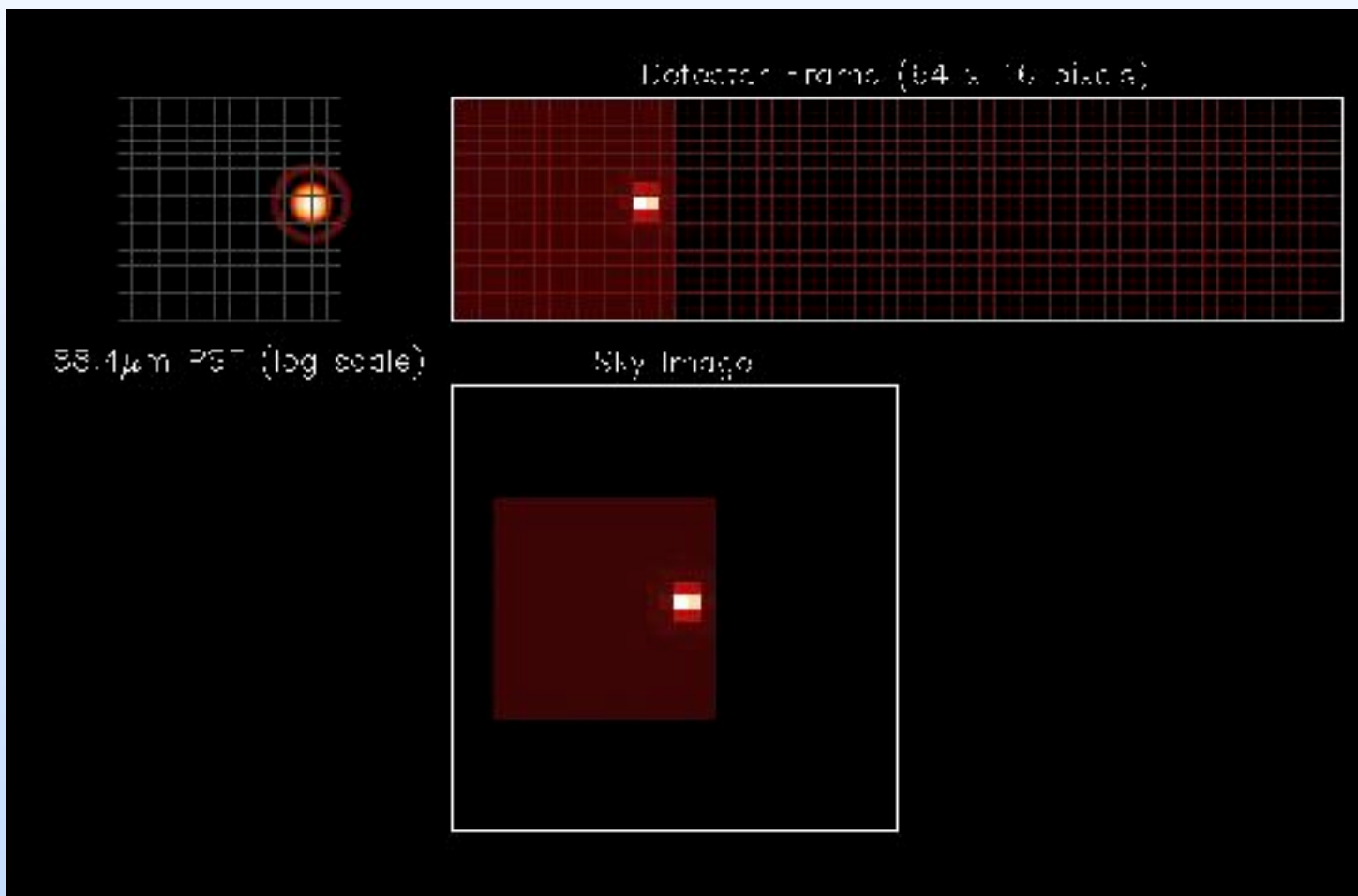
Grating Mode Spectroscopy



The Local Truth: Star Formation and Feedback in the SOFIA Era



Building the Imaging Mode Spectrum



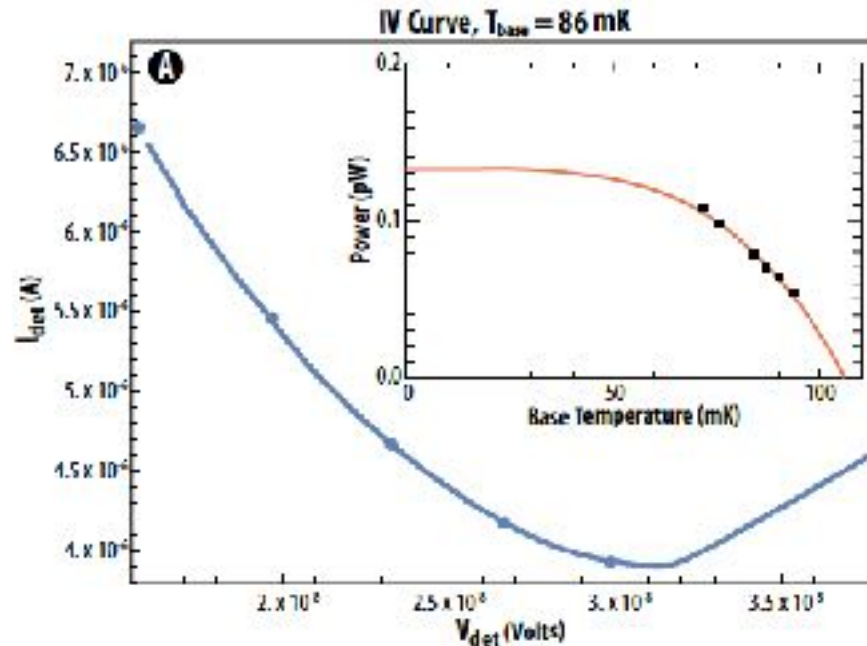
Technical Developments

- Detectors
 - Demonstration of required NEP, plans for flight parts
- Vibrational Heating
 - Approach and design development for a vibration-tolerant system



IV Curve Analysis

- A measured IV curve is shown on the right. The points on the graph indicate bias points where noise measurements were made
- The sweep begins in the linear normal range and proceeds along the hyperbolic path expected in the transition. This is a measured curve, not a fit
- The inset shows the determination of the saturation power, made by taking IV curves at a series of base temperatures.



$P_{sat} : 0.13$ pW
$G(T) = G_0 T^N$
$G_0 : 4.3 \times 10^{-9}$ W/K ⁴
N: 3 (constrained)
$T_c : 106$ mK
$G(T_c) : 5 \times 10^{-12}$ W/K
$R_q : 9.0$ m Ω
$NEP_{photon} : 1.8 \cdot 10^{-18}$ W/ \sqrt{Hz}

- The responsivity of the detector at a given bias point can be accurately derived from the IV curve. This responsivity, combined with the noise spectrum, provides an accurate measure of the detector NEP.

Major Risk in Vibration Immunity

- Based on measured results from the Wisconsin XQC cryostat, we have a design approach and all the tools to design to an operating vibration level
- Our demonstrated dampers provide up to a factor of 100 extra margin
- **Our largest remaining risk is in the definition of the maximum operating vibration level for SOFIA. We must develop this requirement early in the instrument development with the SOFIA program.**

Why Vibrational Heating Now?

- Vibrational heating was not a dominant issue on the Kuiper Airborne Observatory (KAO)
 - Some trouble with microphonic noise pickup
 - No significant effect on cryogenic performance
- The HAWC instrument was designed and built largely by analogy with the KAO instruments, using best practices developed, but not to an operational vibration specification.
 - The user's manual includes a typical vibration spectrum, but there is no "maximum operating environment" and mechanical transfer function for its interpretation.

How is HAWC different?

- HAWC differs from earlier KAO instruments in three ways:
 - It uses an ADR to operate at 200 mK, while the KAO instrument operated at 340 mK using a ^3He evaporation refrigerator
 - The suspended mass of the ADR and detector assembly are significantly higher than those of KAO low temperature instruments.
 - HAWC operates on SOFIA, so the vibration environment may be different.

Vibration Control

- HIRMES will be designed to function at full sensitivity at the vibration level measured in flight on the SOFIA telescope
 - The SOFIA operators manual shows a typical spectrum measured on the FORCAST. In the absence of a formal requirement, we will adopt a provisional requirement of 3 dB higher than the FORCAST in flight measurement. We will work with the SOFIA project to acquire sufficient data to generate a formal requirement which we shall meet prior to delivery
 - Final design must be based on a vibration spec representative of the full range of flight conditions, and thus will depend on the cooperation and participation of the SOFIA project in generating such a spec.
 - We requested a maximum operating vibration spec from the project during the study phase, but it was not available

The HIRMES Approach

- The HIRMES team will design the system *ab initio* to have immunity to vibrational input, and will include eddy current dampers to provide significant additional margin against it.
 - Our development program includes FEM analysis and vibrational tests at the instrument level to assure compliance. We will use small inertial drivers for subsystem tests to minimize risk prior to system integration. The drivers and accelerometers will remain on the instrument and their data logged during the full life of the instrument.

Solving the Problem

- Limiting the coupling to environmental vibration is a well understood engineering problem, and there are examples of its solution.
 - I will focus on a closely related system, the XQC (the X-ray Quantum Calorimeter), a cryogenic rocket instrument operating at 0.050K. It has flown 7 times, and has routinely achieved precision control at 0.05 K within 30 s of launch.
 - The HIRMES PI is a coauthor on the paper describing the vibration mitigation

The Mechanical System

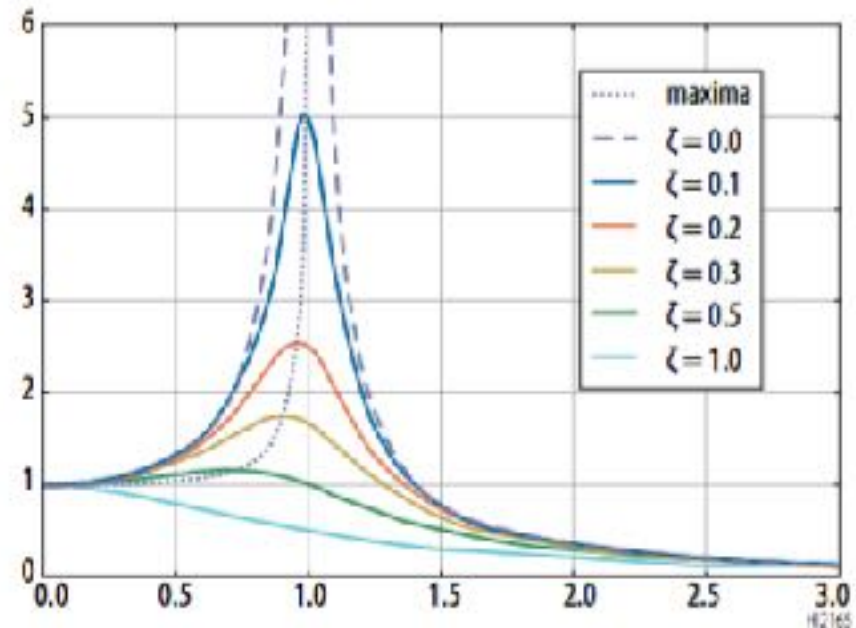
- The detector system is modeled as a harmonic oscillator with damping in its support structure.
- When its base is vibrated, the system oscillates. It reaches equilibrium when the input power to the system is balanced by the dissipation in the structure. The amplitude of oscillation will generally increase until this condition obtains.

Energy Transferred to a Resonator

- When the base of a damped harmonic oscillator is excited by a white noise spectrum, its ultimate dissipation is independent of the Q of the oscillator, and depends only on mass.
- One cannot reduce the coupled power by increasing damping of the support structure, but only by filtering the input spectrum to limit the signal amplitude at the resonant frequency.

Damped Oscillator

- One cannot reduce the coupled power by increasing damping of the resonator, but only by filtering the input spectrum to limit the signal amplitude at the resonant frequency.
- The coupled power is proportional to the suspended mass
 - The HIRMES ADR salt pill is 300g compared to 1.7 kg for HAWC



Design Concept

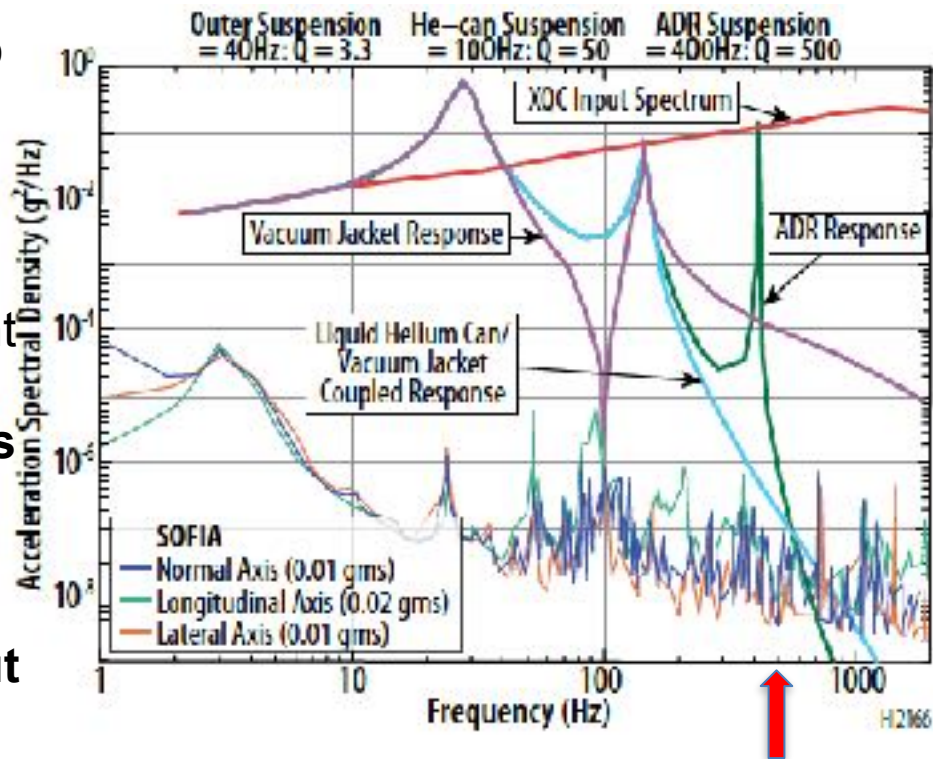
- To reduce the amplitude of vibrational input power at the input to ADR and detector assembly, one must:
 - Place fundamental resonances of cryostat structure at low frequencies (~ 30 Hz)
 - Put the ADR/detector frequency at the highest practical frequency (~ 400 Hz)
 - Put intermediate stages at optimized intermediate frequencies.

Detailed Design Process

- One must carry out a coupled modes analysis to measure the transmission of input vibrational power from the instrument mounting ring to the ADR/Detector mounts
- The parameters that are free for optimization are the frequencies of the optical bench, the 1 K isolation stage, and the 0.05 K detector system

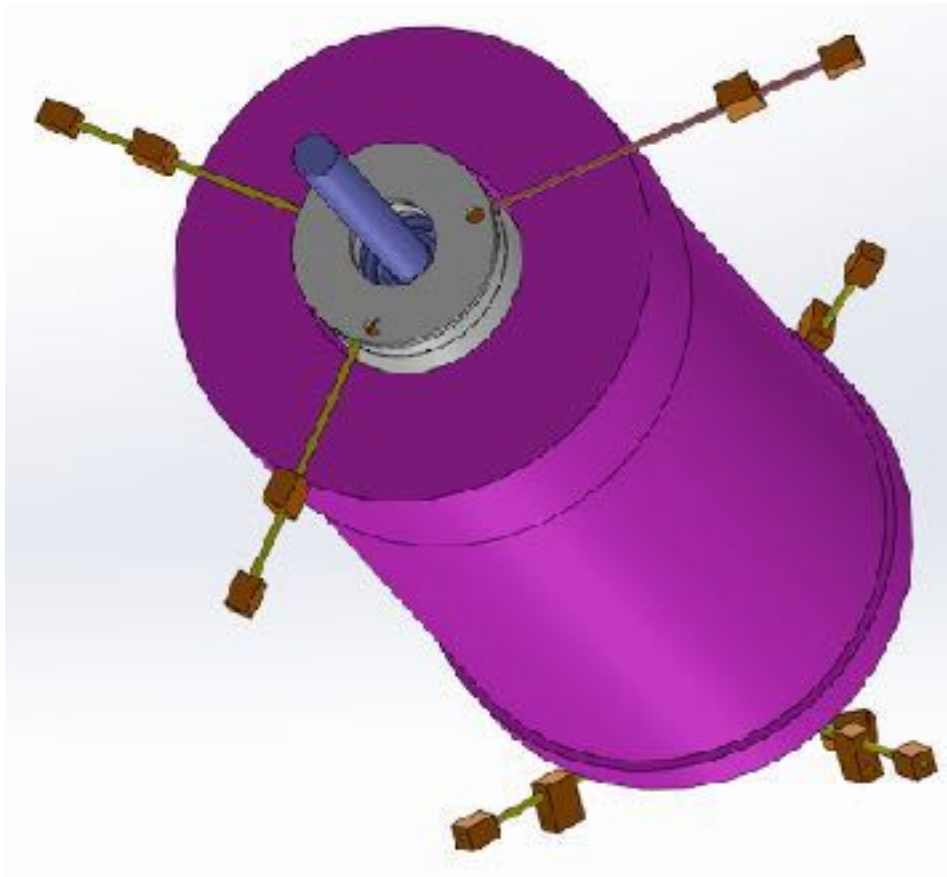
ADR Vibrational Heating

- The cryostat and its support structure can act as a mechanical filter to limit coupling to the low temperature stage
- Vibrational amplitude of ADR was within a factor of two of the model prediction
- Several additional orders of magnitude reduction can be achieved with eddy current damping, described below
- **Based on instrument level vibration tests at Wallops, the Wisconsin ADR would have a factor of $\sim 10^3$ less heating than HAWC+ (scaled to the HAWC+ low temperature mass) given the SOFIA input spectrum (240 μ W for HAWC+, 26 nW predicted for scaled XQC)**
- **Damping will provide at least a factor of 10 extra margin, probably more with design work**

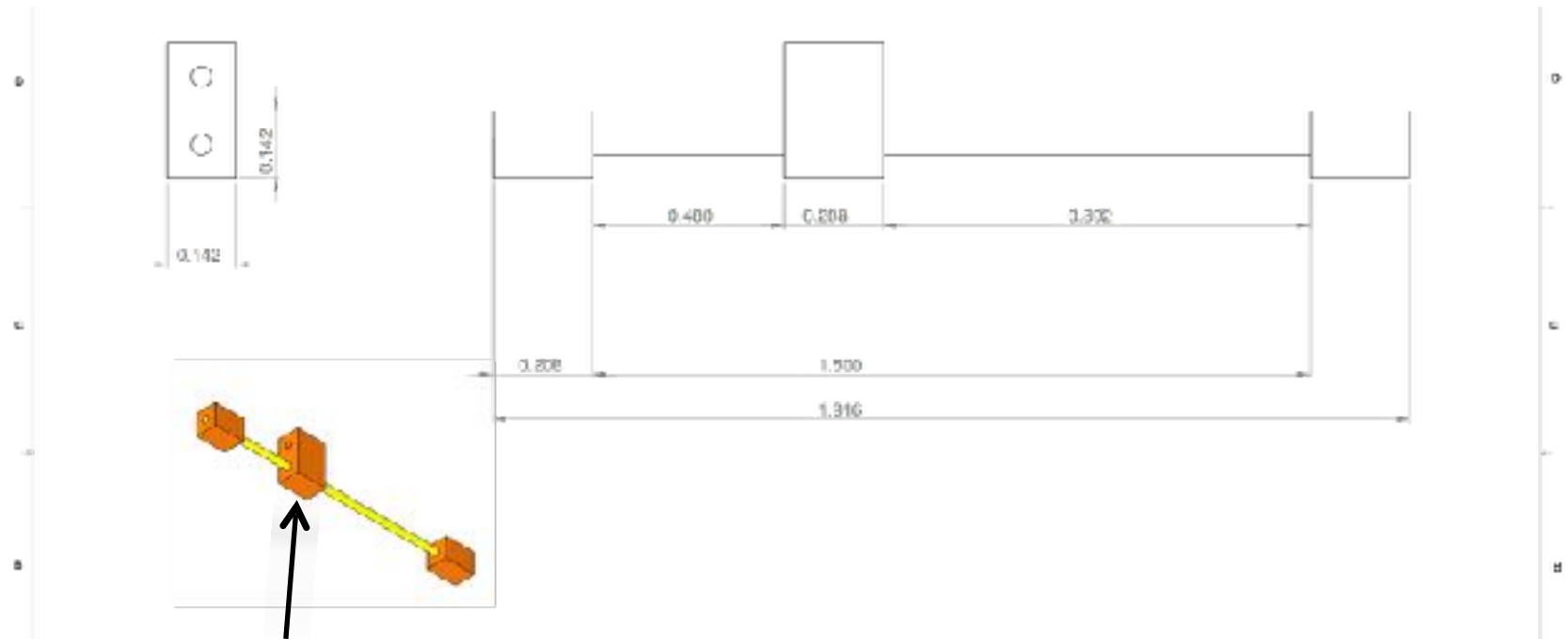


Cui, W., Almy, R., Deiker, S., McCammon, D., Morgenthaler, J., Sanders, W. T., Kelley, R. K., Marshall, F. J., Moseley, S. H., Stahle, C. K., and Szymkowiak, A. E., 1994, SPIE, 2280/363, doi: 10.1117/12.186824.

ADR Magnet, Salt Pill, Inconel Tube, and Inner Kevlar Attachment



Rigid Kevlar Element



Intermediate Heat Sink.
Copper heat strap wire
will be inserted into extra
hole and crimped at
assembly.

		1.001 1.002 1.003 1.004 1.005 1.006 1.007 1.008 1.009 1.010 1.011 1.012 1.013 1.014 1.015 1.016 1.017 1.018 1.019 1.020 1.021 1.022 1.023 1.024 1.025 1.026 1.027 1.028 1.029 1.030 1.031 1.032 1.033 1.034 1.035 1.036 1.037 1.038 1.039 1.040 1.041 1.042 1.043 1.044 1.045 1.046 1.047 1.048 1.049 1.050 1.051 1.052 1.053 1.054 1.055 1.056 1.057 1.058 1.059 1.060 1.061 1.062 1.063 1.064 1.065 1.066 1.067 1.068 1.069 1.070 1.071 1.072 1.073 1.074 1.075 1.076 1.077 1.078 1.079 1.080 1.081 1.082 1.083 1.084 1.085 1.086 1.087 1.088 1.089 1.090 1.091 1.092 1.093 1.094 1.095 1.096 1.097 1.098 1.099 1.100 1.101 1.102 1.103 1.104 1.105 1.106 1.107 1.108 1.109 1.110 1.111 1.112 1.113 1.114 1.115 1.116 1.117 1.118 1.119 1.120 1.121 1.122 1.123 1.124 1.125 1.126 1.127 1.128 1.129 1.130 1.131 1.132 1.133 1.134 1.135 1.136 1.137 1.138 1.139 1.140 1.141 1.142 1.143 1.144 1.145 1.146 1.147 1.148 1.149 1.150 1.151 1.152 1.153 1.154 1.155 1.156 1.157 1.158 1.159 1.160 1.161 1.162 1.163 1.164 1.165 1.166 1.167 1.168 1.169 1.170 1.171 1.172 1.173 1.174 1.175 1.176 1.177 1.178 1.179 1.180 1.181 1.182 1.183 1.184 1.185 1.186 1.187 1.188 1.189 1.190 1.191 1.192 1.193 1.194 1.195 1.196 1.197 1.198 1.199 1.200 1.201 1.202 1.203 1.204 1.205 1.206 1.207 1.208 1.209 1.210 1.211 1.212 1.213 1.214 1.215 1.216 1.217 1.218 1.219 1.220 1.221 1.222 1.223 1.224 1.225 1.226 1.227 1.228 1.229 1.230 1.231 1.232 1.233 1.234 1.235 1.236 1.237 1.238 1.239 1.240 1.241 1.242 1.243 1.244 1.245 1.246 1.247 1.248 1.249 1.250 1.251 1.252 1.253 1.254 1.255 1.256 1.257 1.258 1.259 1.260 1.261 1.262 1.263 1.264 1.265 1.266 1.267 1.268 1.269 1.270 1.271 1.272 1.273 1.274 1.275 1.276 1.277 1.278 1.279 1.280 1.281 1.282 1.283 1.284 1.285 1.286 1.287 1.288 1.289 1.290 1.291 1.292 1.293 1.294 1.295 1.296 1.297 1.298 1.299 1.300 1.301 1.302 1.303 1.304 1.305 1.306 1.307 1.308 1.309 1.310 1.311 1.312 1.313 1.314 1.315 1.316 1.317 1.318 1.319 1.320 1.321 1.322 1.323 1.324 1.325 1.326 1.327 1.328 1.329 1.330 1.331 1.332 1.333 1.334 1.335 1.336 1.337 1.338 1.339 1.340 1.341 1.342 1.343 1.344 1.345 1.346 1.347 1.348 1.349 1.350 1.351 1.352 1.353 1.354 1.355 1.356 1.357 1.358 1.359 1.360 1.361 1.362 1.363 1.364 1.365 1.366 1.367 1.368 1.369 1.370 1.371 1.372 1.373 1.374 1.375 1.376 1.377 1.378 1.379 1.380 1.381 1.382 1.383 1.384 1.385 1.386 1.387 1.388 1.389 1.390 1.391 1.392 1.393 1.394 1.395 1.396 1.397 1.398 1.399 1.400 1.401 1.402 1.403 1.404 1.405 1.406 1.407 1.408 1.409 1.410 1.411 1.412 1.413 1.414 1.415 1.416 1.417 1.418 1.419 1.420 1.421 1.422 1.423 1.424 1.425 1.426 1.427 1.428 1.429 1.430 1.431 1.432 1.433 1.434 1.435 1.436 1.437 1.438 1.439 1.440 1.441 1.442 1.443 1.444 1.445 1.446 1.447 1.448 1.449 1.450 1.451 1.452 1.453 1.454 1.455 1.456 1.457 1.458 1.459 1.460 1.461 1.462 1.463 1.464 1.465 1.466 1.467 1.468 1.469 1.470 1.471 1.472 1.473 1.474 1.475 1.476 1.477 1.478 1.479 1.480 1.481 1.482 1.483 1.484 1.485 1.486 1.487 1.488 1.489 1.490 1.491 1.492 1.493 1.494 1.495 1.496 1.497 1.498 1.499 1.500	DATE GMN 8/16/2011 CHECKED SEC APP REV APP Q.A. DRAWING	GMN NEON engineering TRC SEC: URS, NJ. B. David Kessler, P.E.
--	--	--	---	--

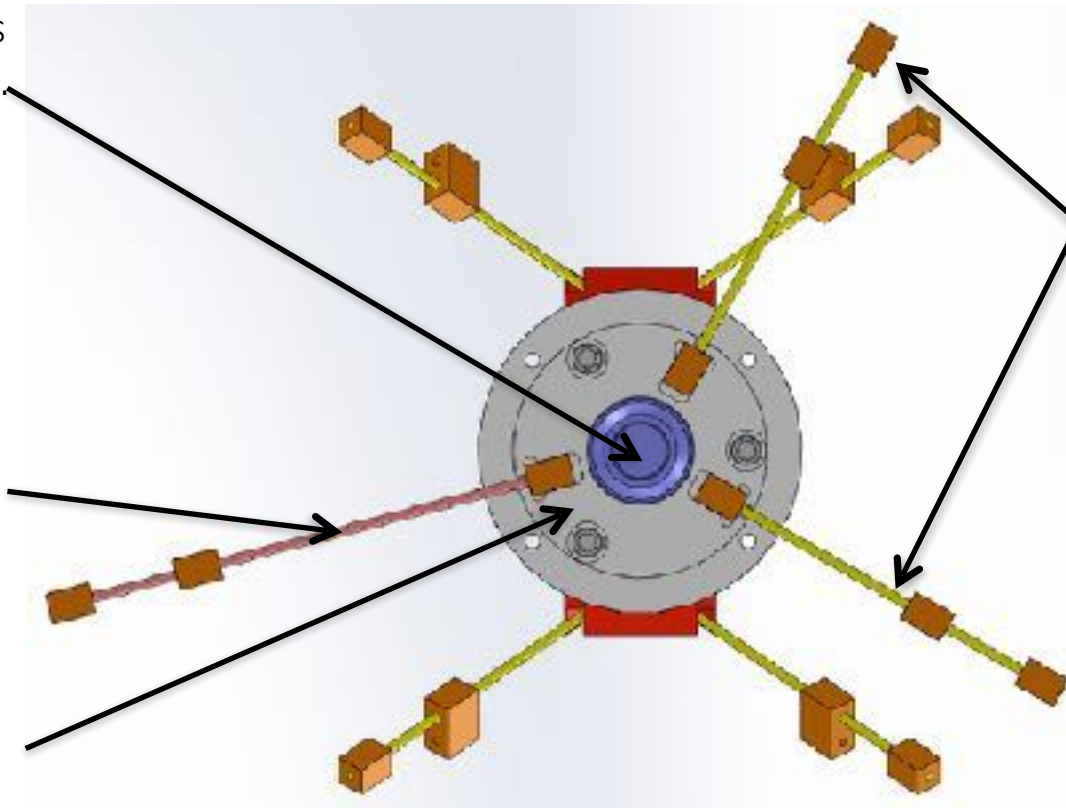
2 Degree Of Constraint (DOC) End Detail

Salt pill thermal bus comes out this end.

2 Rigid Kevlar elements at 90°

Preload Kevlar at 135°

Kevlar swage retainer cap removed for clarity

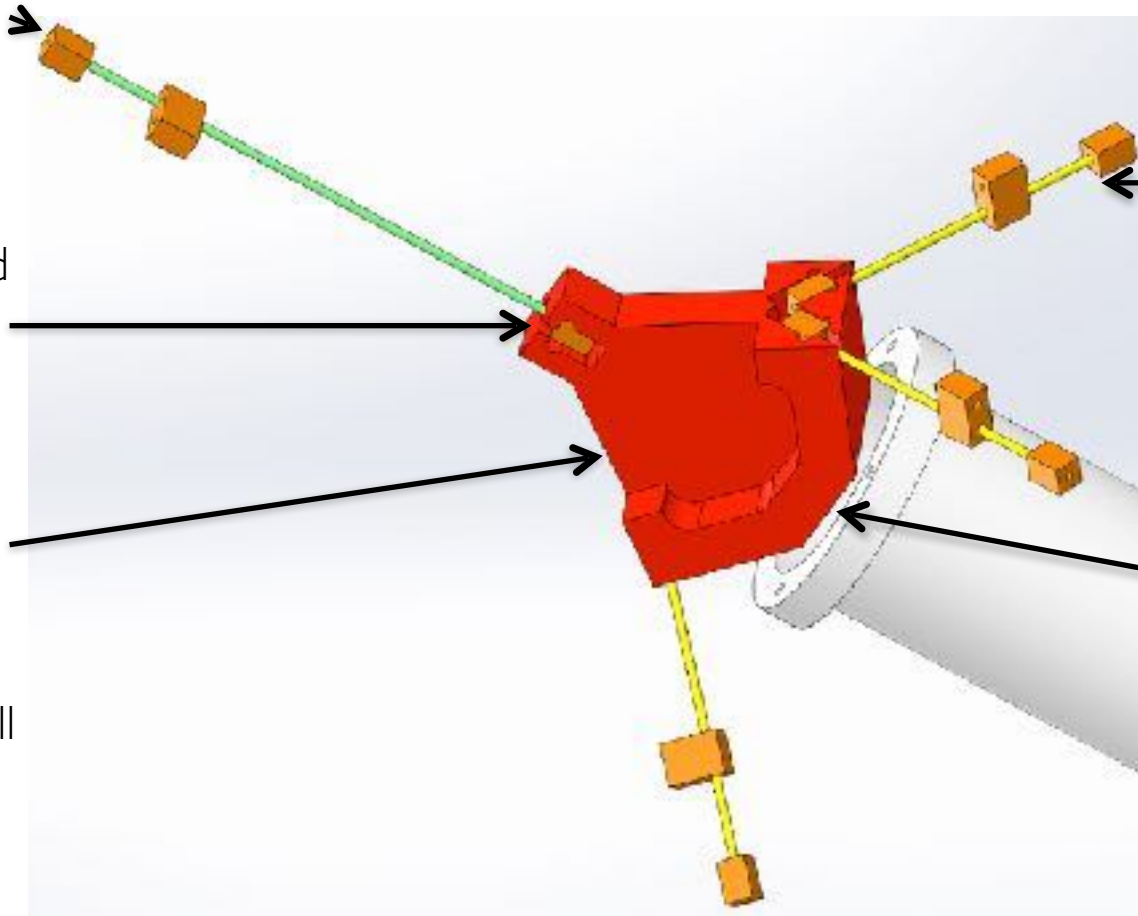


4 DOC End

Axial preload
Kevlar is
"longer"

Kevlar swages
will be retained
by caps screwed
in place.

4 DOC fitting is
"relatively" easy
to machine,
compound
Kevlar angles will
be
straightforward
to measure.

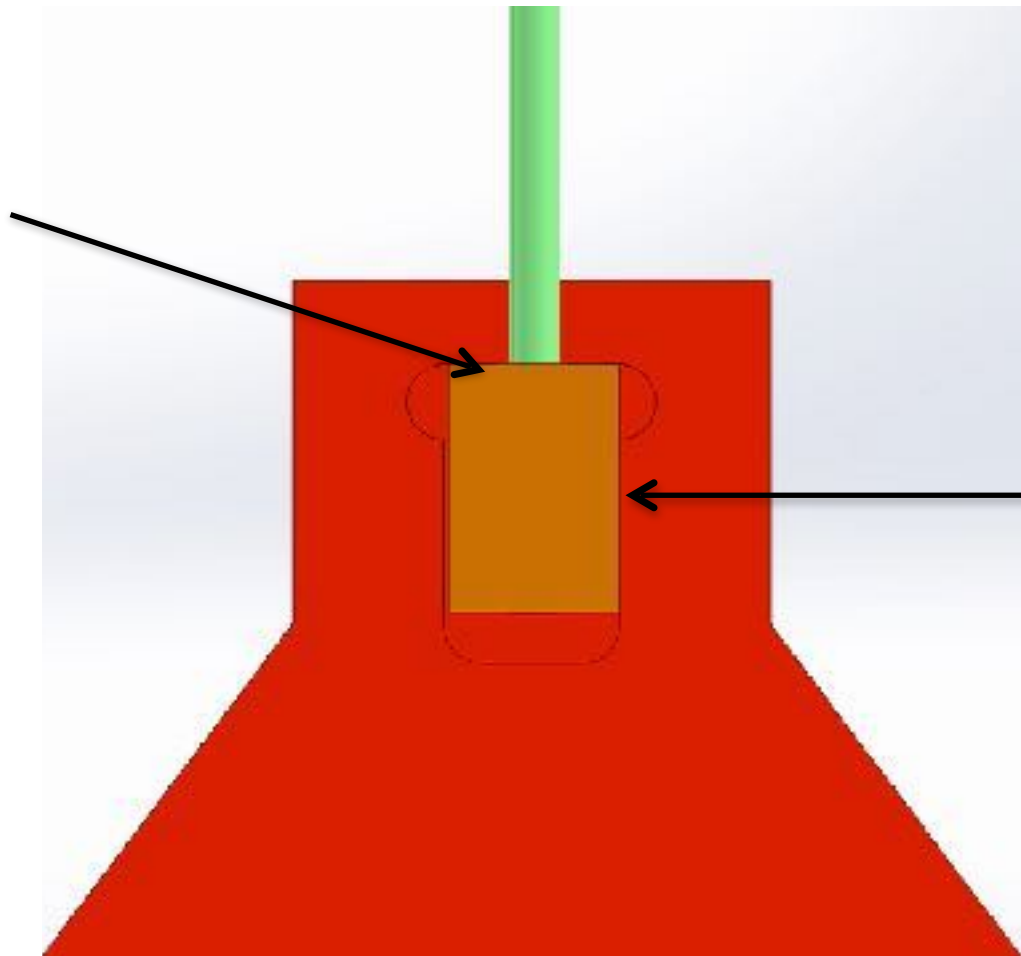


Kevlar element
length (and thus
salt pill position)
adjustment will be
by means of shims
at the outboard
ends.

Not attached to
Inconel tube yet,
awaiting feedback
on concept.

Detail of Kevlar Swage Fitting

Bearing Surface



Location and alignment surfaces

XQC Thermal Performance

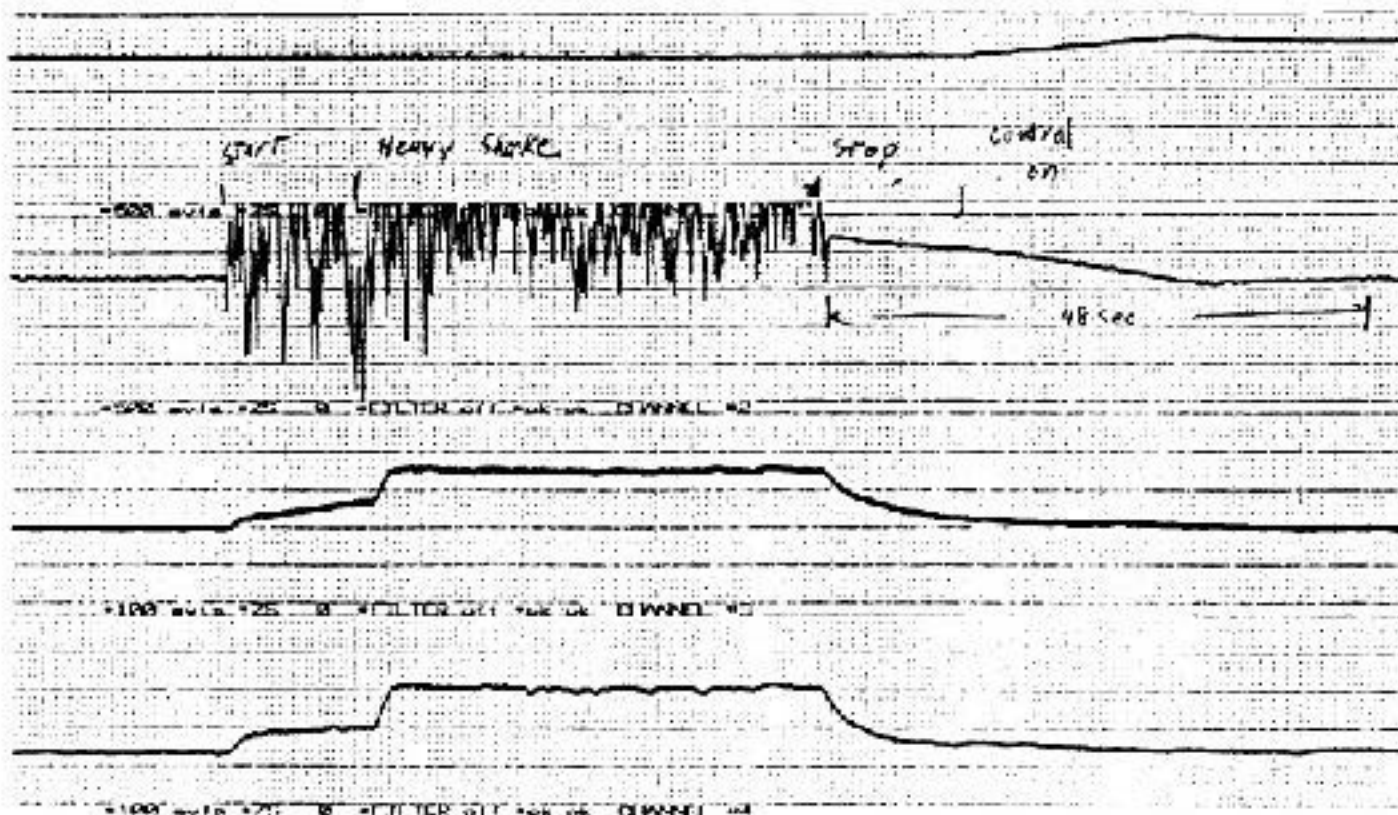


Figure 5: Chart record of coldplate temperature during “simulated flight” vibration test at Wallops Flight Facility. Temperature returns to within 5 μ K of the 65 mK setpoint about 48 seconds after end of powered flight.

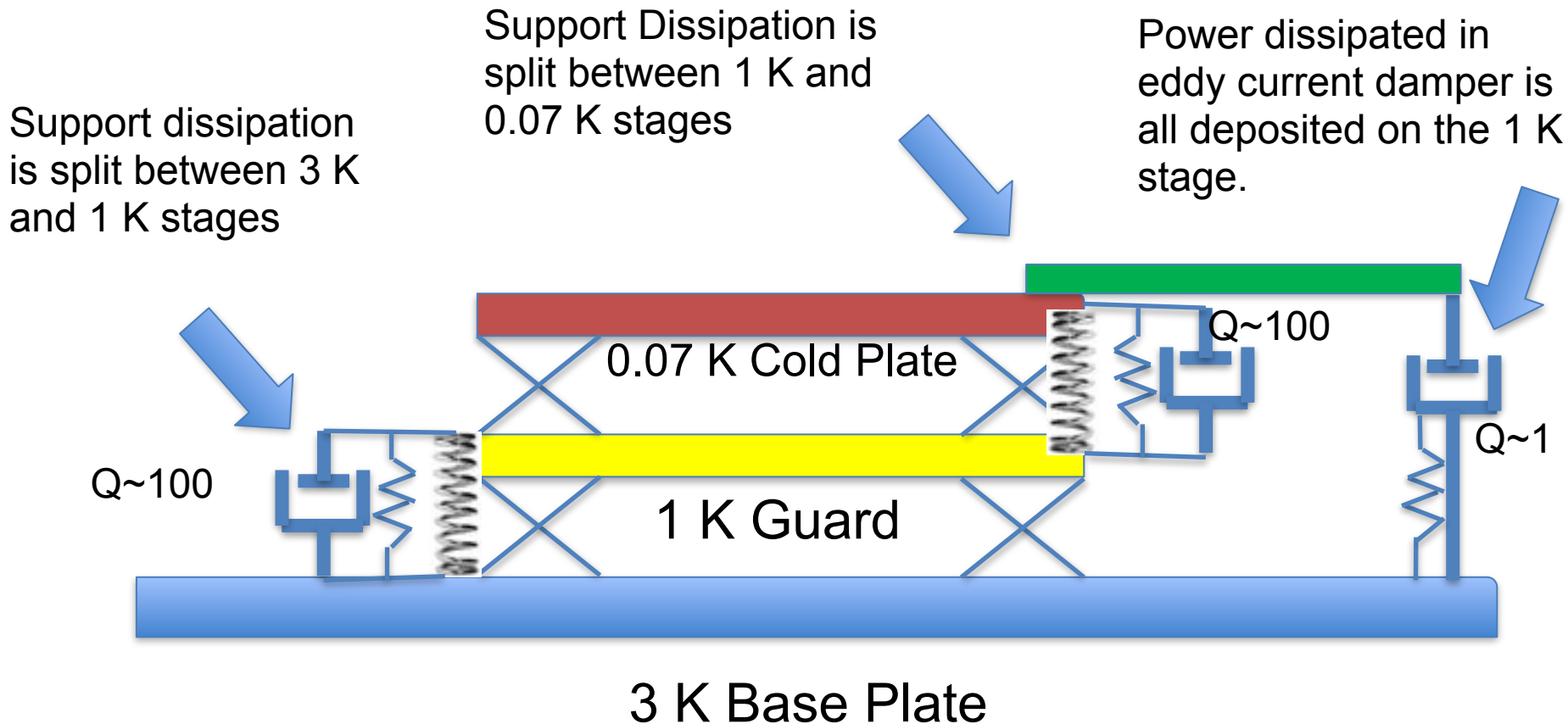
Vibrational Heating Mitigation on Astro-H

- The Astro-H detectors had significant additional noise due to heating from the cryocooler compressor vibration
 - They were bolted to the dewar shell
- This was mitigated by designing external damping systems for the compressors. The mitigation completely eliminated the problem
- The HIRMES PI was involved in the analysis of the heating problem and in developing mitigation approaches
- **Vibration isolation is a solvable engineering problem given the input spectrum and the allowable response.**

Damping

- The mechanical loss (damping) of typical cryogenic structures is small, with tensile Kevlar cryogenic suspensions providing quality factors (Q) ranging from 50 – 400.
- Application of damping can greatly reduce the amplitude of the vibrations
 - If the damped power is dissipated on the ADR/ Detector stage, there is no reduction in heating
 - If the power can be dissipated on another stage with more cooling power, this eliminates much of the heating on the low temperature stage.

Damping in Cryogenic Systems

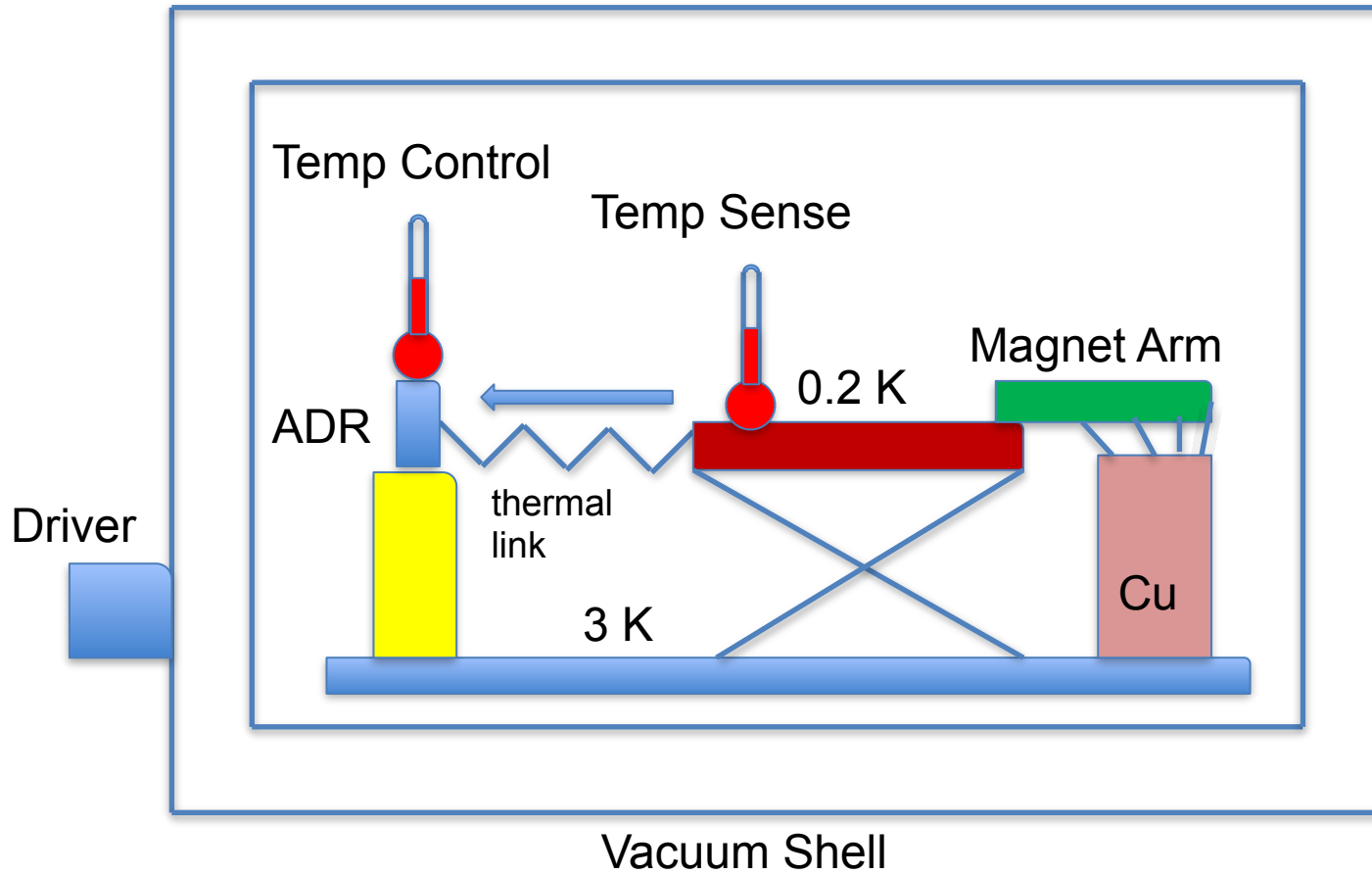


The eddy current damping constant dominates that of the support structure, so most (>99%) of the dissipated power can be directed to the 3 K plate.

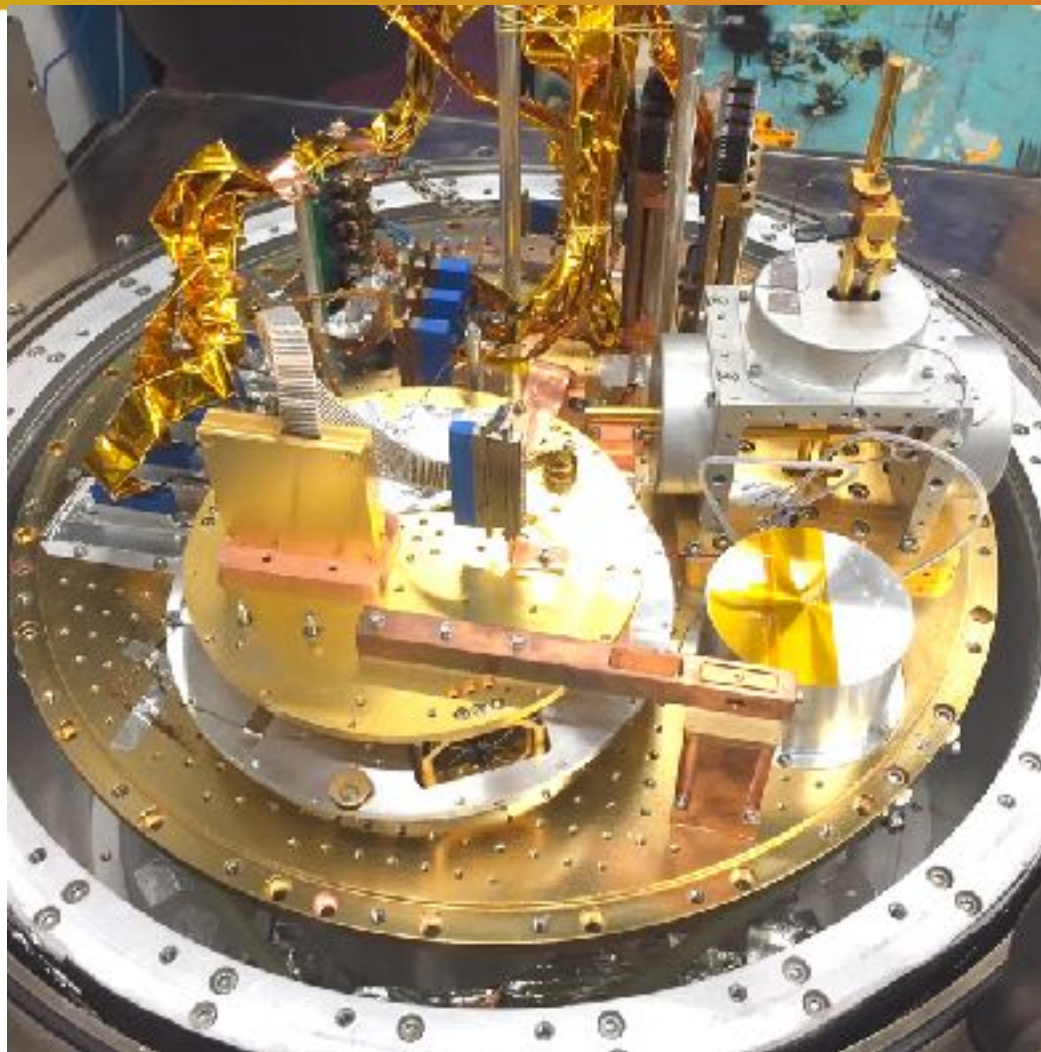
Magnetic Damping

- Eddy current damping is an excellent mechanism for low temperature damping.
 - Passive
 - Improves linearly with metallic conductivity
- We have developed a design using multipole magnets that provide excellent damping.
 - The high order multipole field decays rapidly
 - Residual field can be eliminated using Cryoperm or other low temperature permeable shield materials

Experimental Setup

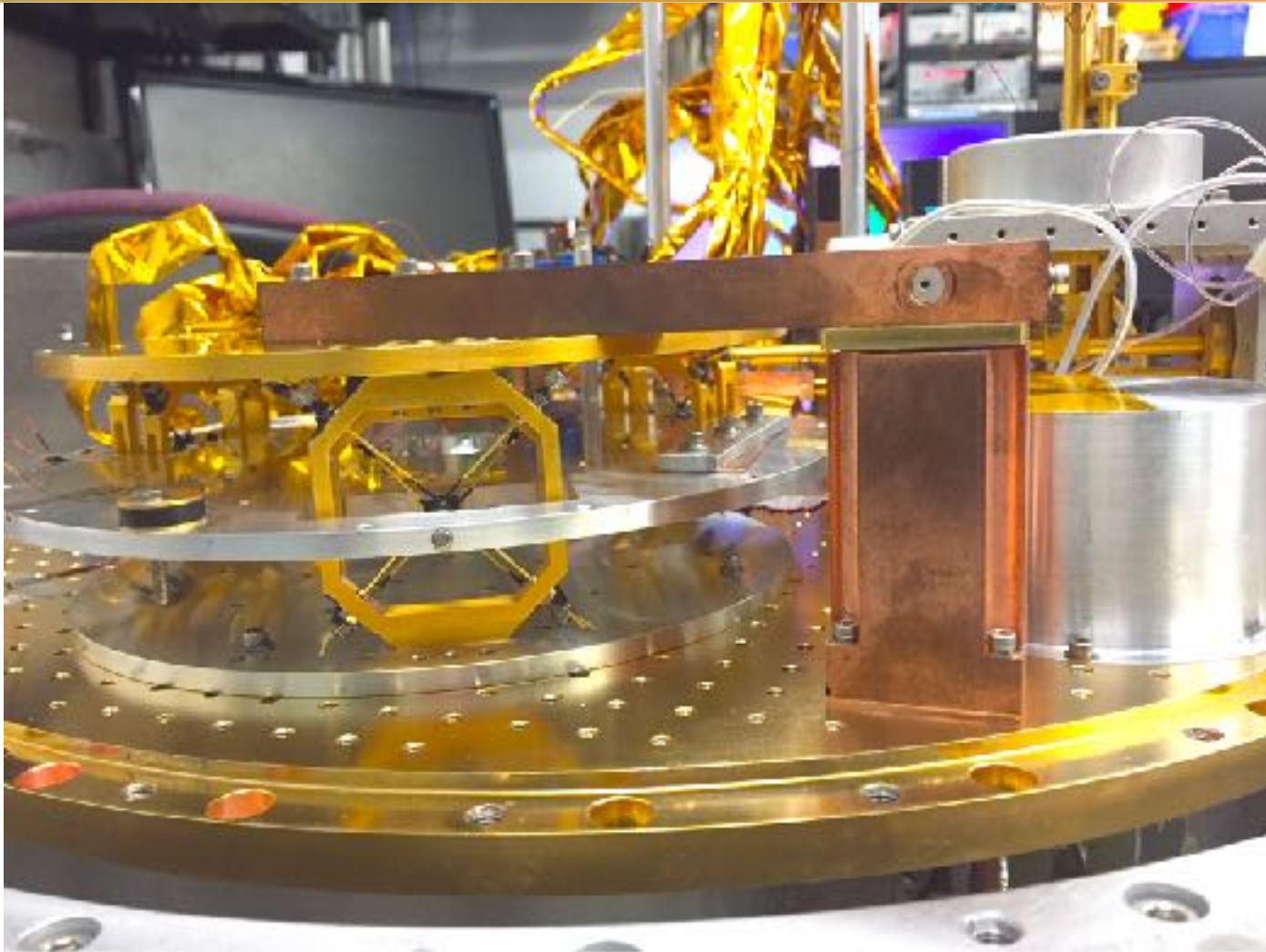


Heating Test Configuration



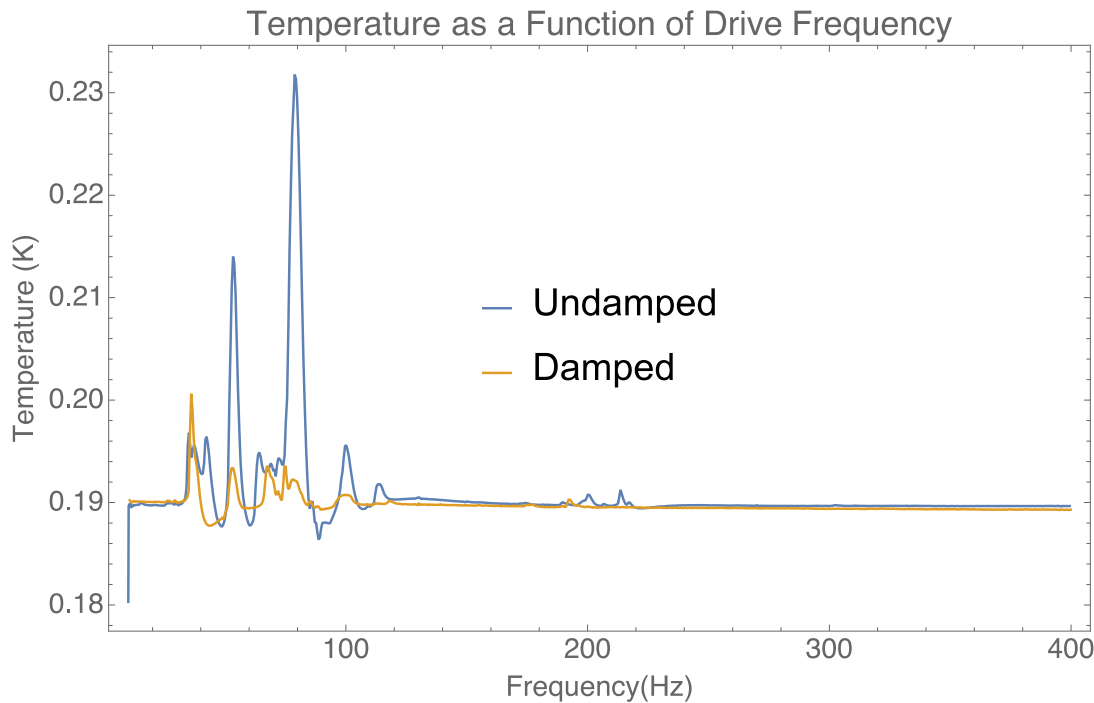
High Resolution Mid-infrared Spectrometer

Heating Test Configuration



High Resolution Mid-infrared Spectrometer

Magnetic Damping Greatly Reduces Vibrational Heating



- Initial test of partially damped system
- No damper on 1 K stage



ADR Vibration Summary

- We are including vibration control in the design from the beginning. Proper design, demonstrated on XQC, will provide a robust design for SOFIA operation.
- GSFC has the experience and expertise from XQC and Astro-H to address this problem.
- Given the SOFIA vibration level in the Vibration and Dynamic Environment section in the SI Developers Handbook (measured with FORCAST mounted), our design will provide significant margin.

Schedule

- PDR: Documents
 - Technical
 - CDR:
 - I&T at GSFC:
 - Delivery to Armstrong:
 - First Flights:
 - Re-introduce selves to families:
- November 2016
Jan 2017
May 2017
November 2017
December 2018
Spring 2019
Summer 2019



Thanks!



GTO Observing Program

Table D-1: GTO Observing Program Targets (observing times are calculated based on $1 \times 10^{-17} \text{ W m}^{-2} \text{ 5}\sigma$ in 1 hour)*.

Program	Intensity (W/m ²)	SNR	Total time with overhead (hours)
Optimal H₂¹⁶O water lines for Protoplanetary disks with HIRMES (transition/wavelength μm)			
4 4 0 -> 3 1 3 (28.914)	3.10E-17	27.00	4.5
6 4 3 -> 6 1 6 (32.313)	3.30E-17	29.00	4.5
6 5 1 -> 6 2 4 (34.987)	2.20E-17	19.00	4.5
Subtotal			13.5
H₂O vapor targets			
RNO 90	3.10E-17	26.85	4.5
AS 205	4.96E-17	35.07	3
HD 163296	3.10E-17	31.00	6
Subtotal			13.5
Targets (HD (1-0) transition)			
HD 163296	1.00E-17	21.7	5
TW Hya	5.00E-18	17.5	10
Subtotal			15

[OI] 63 μm targets			
RNO 90	1.29E-16	45.61	0.75
AS 205	2.15E-16	76.01	0.75
HD 163296	2.08E-16	73.68	0.75
TW Hya	3.65E-17	12.90	1.5
Subtotal			3.75
H₂O ice targets **		Flux density (Jy)	
RNO 90	3.2	64.0	0.75
AS 205	15.5	310.0	0.75
HD 163296	17	340.0	0.75
TW Hya	2.5	50.0	0.75
Subtotal			3
Total Time			48.75
*The expected performance is significantly better (depending on the line), e.g., the observing time gain margin for HD, H ₂ O and [OI] lines are 7.3, 16.0 and 2.5, respectively.			
** Smoothed down to 1 μm resolution.			

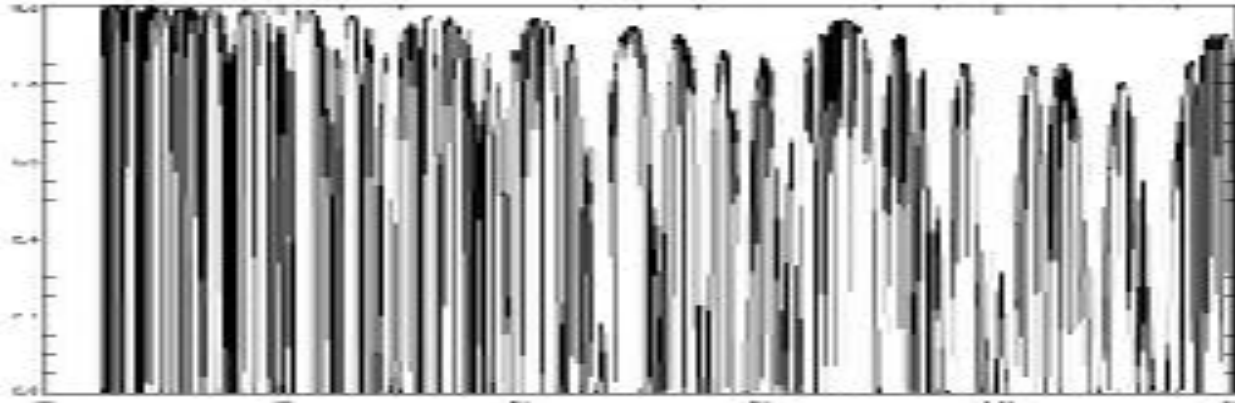


HIRMES Instrument Specification

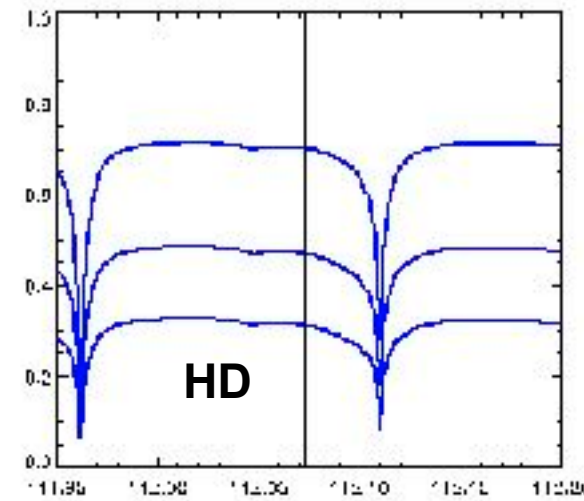
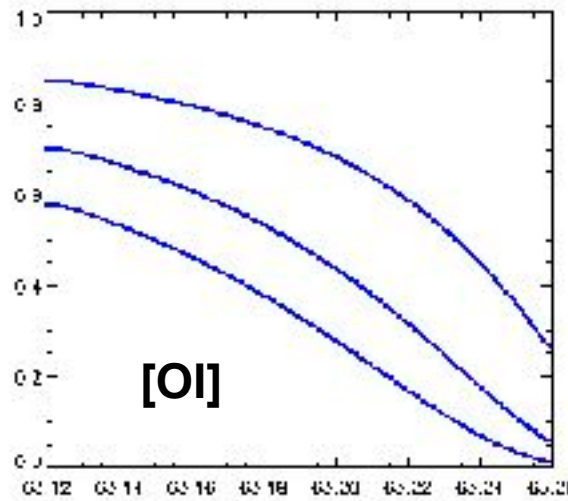
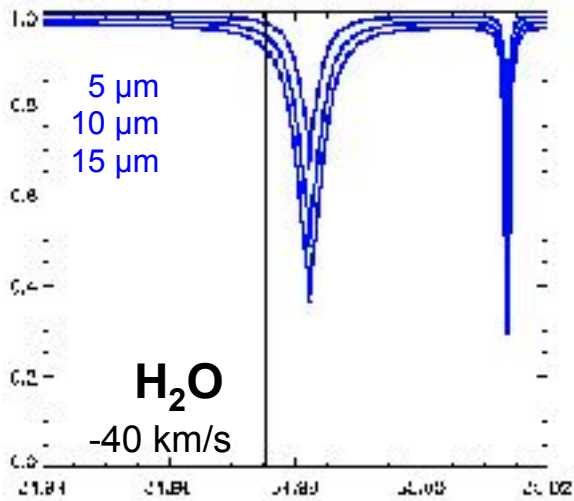
Parameters	Note
Sensitivity (5σ , 1 hour)	$3 \times 10^{-18} \text{ W/m}^2$
Resolving power	$\lambda/\Delta\lambda \sim 100,000(\text{high}) ; 19,000 (\text{mid}); 600(\text{low})$
Angular resolution	Diffraction limited @ $\lambda=45 \mu\text{m}$
Spectral range	25-122 μm
Number of det. modules	2
Detector format	16 x 64 mid/low-res, 8x16 high-res
Detector technology & operating temperature	TES bolometers @ 0.1 K
Detector sensitivity	NEP $\sim 1 \times 10^{-18} \text{ W}/\sqrt{\text{Hz}}$ including photon noise
Detector cold readout	SQUID
Detector warm readout	UBC Multichannel Electronics (MCE)
Cooler	Pulse tube cooler and adiabatic demagnetization refrigerator (ADR)



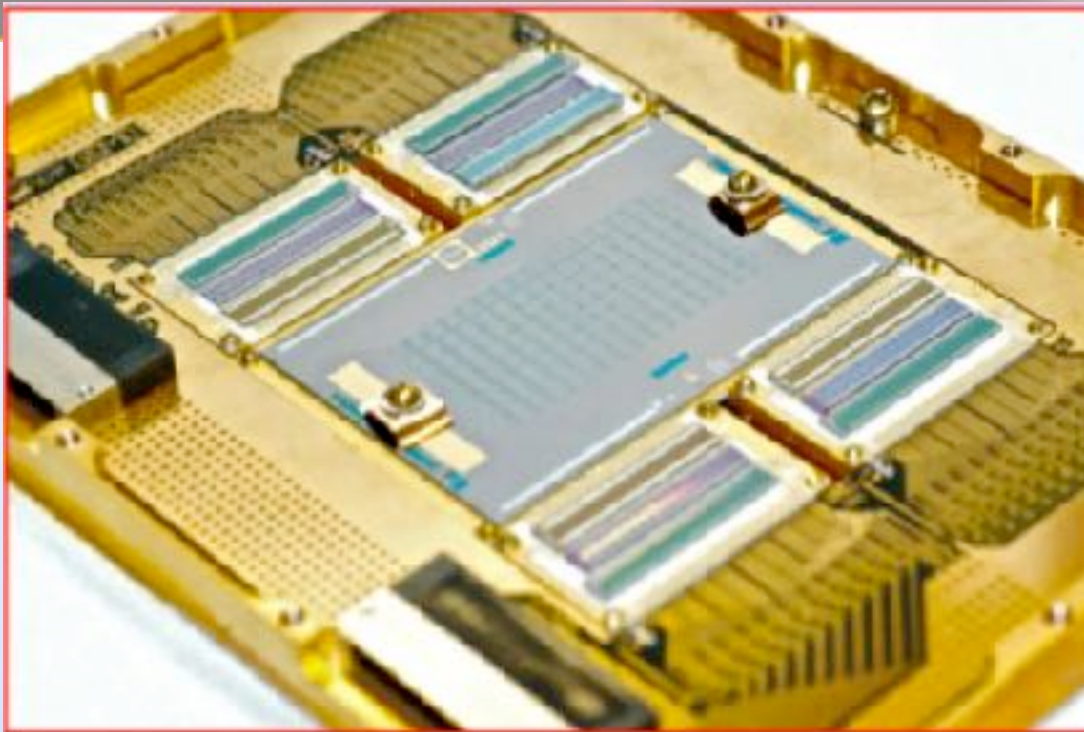
Atmospheric transmission



ATRAN Model Input Parameters
 Observatory Altitude: 41000 feet
 Observatory Latitude: 30 degrees
 Water Vapor Overburden: 10 microns
 Std Atmosphere with : 2 Layers
 Zenith Angle: 45 degrees



HIRMES detector assembly



Shown is an 8x16 array of 2-mm pixels. HIRMES will have 8x16 and 16x64 arrays of 1-mm pixels in a similar design modular package.